AGU PUBLICATIONS

JGR

Journal of Geophysical Research: Oceans

RESEARCH ARTICLE

10.1002/2014JC010457

Investigation of interbasin exchange and interannual variability in Lake Erie using an unstructured-grid hydrodynamic model

Qianru Niu[1], Meng Xia[1], Edward S. Rutherford[2], Doran M. Mason[2], Eric J. Anderson[2], and David J. Schwab[3]

[1]Department of Natural Sciences, University of Maryland Eastern Shore, Princess Anne, Maryland, USA, [2]NOAA Great Lakes Environmental Research Laboratory, Ann Arbor, Michigan, USA, [3]Graham Environmental Sustainability Institute, U-M Water Center, University of Michigan, Ann Arbor, Michigan, USA

Key Points:
- Hydraulic and density flows both dominate interbasin water exchange
- Interannual variability is dominated by atmospheric forcing
- Dominant mechanisms of interbasin water exchange vary interseasonally

Correspondence to:
M. Xia,
mxia@umes.edu

Citation:
Niu, Q., M. Xia, E. S. Rutherford, D. M. Mason, E. J. Anderson, and D. J. Schwab (2015), Investigation of interbasin exchange and interannual variability in Lake Erie using an unstructured-grid hydrodynamic model, *J. Geophys. Res. Oceans*, *120*, 2212–2232, doi:10.1002/2014JC010457.

Received 13 OCT 2014
Accepted 17 FEB 2015
Accepted article online 20 FEB 2015
Published online 27 MAR 2015

Abstract Interbasin exchange and interannual variability in Lake Erie's three basins are investigated with the help of a three-dimensional unstructured-grid-based Finite Volume Coastal Ocean Model (FVCOM). Experiments were carried out to investigate the influence of grid resolutions and different sources of wind forcing on the lake dynamics. Based on the calibrated model, we investigated the sensitivity of lake dynamics to major external forcing, and seasonal climatological circulation patterns are presented and compared with the observational data and existing model results. It was found that water exchange between the western basin (WB) and the central basin (CB) was mainly driven by hydraulic and density-driven flows, while density-driven flows dominate the interaction between the CB and the eastern basin (EB). River-induced hydraulic flows magnify the eastward water exchange and impede the westward one. Surface wind forcing shifts the pathway of hydraulic flows in the WB, determines the gyre pattern in the CB, contributes to thermal mixing, and magnifies interbasin water exchange during winter. Interannual variability is mainly driven by the differences in atmospheric forcing, and is most prominent in the CB.

1. Introduction

Three distinct geographic basins characterize Lake Erie: the shallow (mean depth 7.4 m) and relatively flat western basin (WB); the central basin (CB) with extremely flat topography (mean depth 18.5 m); and the deep and steep eastern basin (EB; mean depth 24.4 m) with maximum depth of 64 m (Figure 1) [*Bolsenga and Herdendorf*, 1993]. Lake hydrodynamics have recently received increased attention because of the concerns from the intermittent occurrences of harmful algal blooms in the WB and hypoxia in the CB [*Lam and Schertzer*, 1987; *Michalak et al.*, 2013], and the importance of limnetic physics in determining their causes, distributions, frequencies, and outcomes [*Rao et al.*, 2008; *Schwab et al.*, 2009].

Water masses in the three different basins of Lake Erie have distinct physical and biochemical characteristics, such as epilimnetic and hypolimnetic water temperature, dissolved oxygen, and nutrient concentrations [*Schertzer et al.*, 1987; *Bolsenga and Herdendorf*, 1993]. Subsequently, the water exchanges between three basins have a significant impact on the lake's biochemical and ecological dynamics. A typical example is the transport of the hypolimnetic water from the EB to the CB, which is recognized as an important source for oxygen renewal in the hypolimnion of the CB [*Lam and Schertzer*, 1987]. *Bartish* [1987] gave a review of the major interbasin exchange mechanisms in Lake Erie, and pointed that the water exchange between the WB and CB is possibly dominated by the hydraulic gradient instead of wind forcing or baroclinic processes based on the observations of *Saylor and Miller* [1987]. The exchange between the CB and EB is likely to be mainly driven by the surface pressure gradient, based on the tracing of water temperature and oxygen concentrations along the intersection of the two basins [*Boyce et al.*, 1980; *Chiocchio*, 1981]. Even though these studies provided insight into dynamics of interbasin water exchanges, these conclusions were drawn based on limited observations [e.g., *Boyce et al.*, 1980; *Bartish*, 1984; *Chiocchio*, 1981; *Saylor and Miller*, 1987], and the results of simple numerical models [e.g., *Gedney and Lick*, 1972]. The relative contributions of the investigated mechanisms remain unknown, and several questions still remain. For example, how large is the eastward movement from the CB to the EB? And, how much water transport from the CB to the WB occurs north of Pelee Island compared to the southern passages and what mechanisms are responsible for the distribution?

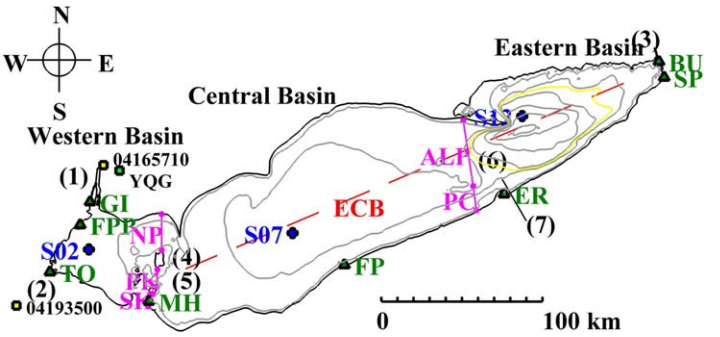

Figure 1. Lake bathymetry, critical geographic names, and observational data locations. Green triangles: water elevation gauges; blue circles: temperature and current observations in 2005; green square: surface weather station YQG (Windsor, Ontario); yellow squares: USGS stations (04165710 at Fort Wayne of Detroit, Michigan, and 04193500 at Waterville, Ohio). Red-dotted line shows model transect ECB. Pink lines represent transects used for calculation of interbasin water exchanges. Isobaths are shown every 10 m, and the yellow contour line stands for the 25 m isobath. Geographic names include: (1) the Detroit River, (2) the Maumee River, (3) the Niagara River, (4) the Pelee Island, (5) the Kelly Island, (6) the Long Point Ridge, and (7) the Pennsylvania Channel.

Concerns over the potential effect of climate change on dynamics in the Great lakes [*Lam and Schertzer*, 1999] have stimulated investigations of interannual variability of the lake dynamics [*Beletsky et al*., 2006; *Austin and Colman*, 2008; *Bennington et al*., 2010], and indicated that the significance of the interannual variability in lake dynamics varies across the Great Lakes. Even though interannual variability has been discussed for Lake Superior [*Bennington et al*., 2010] and Lake Michigan [*Beletsky et al*., 2006], not much work has been done on the dynamically quasi-isolated Lake Erie basins, while significant differences in the interannual variability of its three basins are expected. Taking a view of dynamics in a longer time scale, it has been recognized that the climatological circulation patterns are critical for water quality and ecosystem dynamics around the Great Lakes [*Beletsky and Schwab*, 2008]. Even though there is a considerable history of hydrodynamic modeling for Lake Erie [e.g., *Schwab*, 1978; *Lam and Schertzer*, 1987; *Schwab and Bedford*, 1994; *León et al*., 2005; *Beletsky et al*., 2013], large-scale dynamics in the lake over a long-term time scale, including the interannual variability and interbasin water exchange, have not been sufficiently investigated. *Beletsky et al*. [2013] studied the role of surface wind forcing in the lake dynamics. Their study focused on the dynamics during summer, and was mostly limited to the CB. Though *Bai et al*. [2013] discussed the seasonal climatological circulation in Lake Erie, their study was focus on the whole Great Lakes, and underestimated the river inflow from the Detroit River.

Over the past decade, a Finite Volume Coastal Ocean Model (FVCOM) [*Chen et al*., 2006] has been successfully applied for uses in both the Great Lakes [e.g., *Shore*, 2009; *Anderson et al*., 2010; *Anderson and Schwab*, 2013; *Bai et al*., 2013; *Wilson et al*., 2013] and coastal oceans [e.g., *Chen et al*., 2011; *Beardsley et al*., 2013]. The present work focuses on the general hydrodynamics, including the mechanisms of the interbasin water exchange and interannual variability, based on the model calibration of horizontal and vertical grid resolutions and various wind sources. Our specific objectives are: (1) to evaluate the sensitivity of hydrodynamics in Lake Erie to major external forcing, including river inflows, surface heat flux, and surface wind forcing; (2) to investigate the dynamics and the dominant mechanisms of the interbasin water exchanges among three basins in the lake; and (3) to investigate the driving mechanisms of interannual variability in the lake dynamics, and present climatological circulation maps of the lake with more refined grid resolution and more accurate boundary conditions.

2. Methodology

2.1. Model

FVCOM is a free surface, three-dimensional, primitive equation coastal model with second-order accuracy [*Chen et al*., 2006]. It uses an unstructured triangular grid in the horizontal direction and sigma coordinate in the vertical direction, and thus can adequately resolve coastlines and coastal bathymetry. The finite-volume algorithm incorporated in FVCOM combines the flexibility of geometric fitting of finite-element models and computational efficiency of finite-difference models [*Chen et al*., 2007]. Modified Mellor and Yamada level 2.5b (MY-2.5) and Smagorinsky turbulent closure parameterization [*Mellor and Yamada*, 1982; *Galperin et al*., 1988; *Smagorinsky*, 1963] are included to calculate vertical and horizontal mixing, respectively.

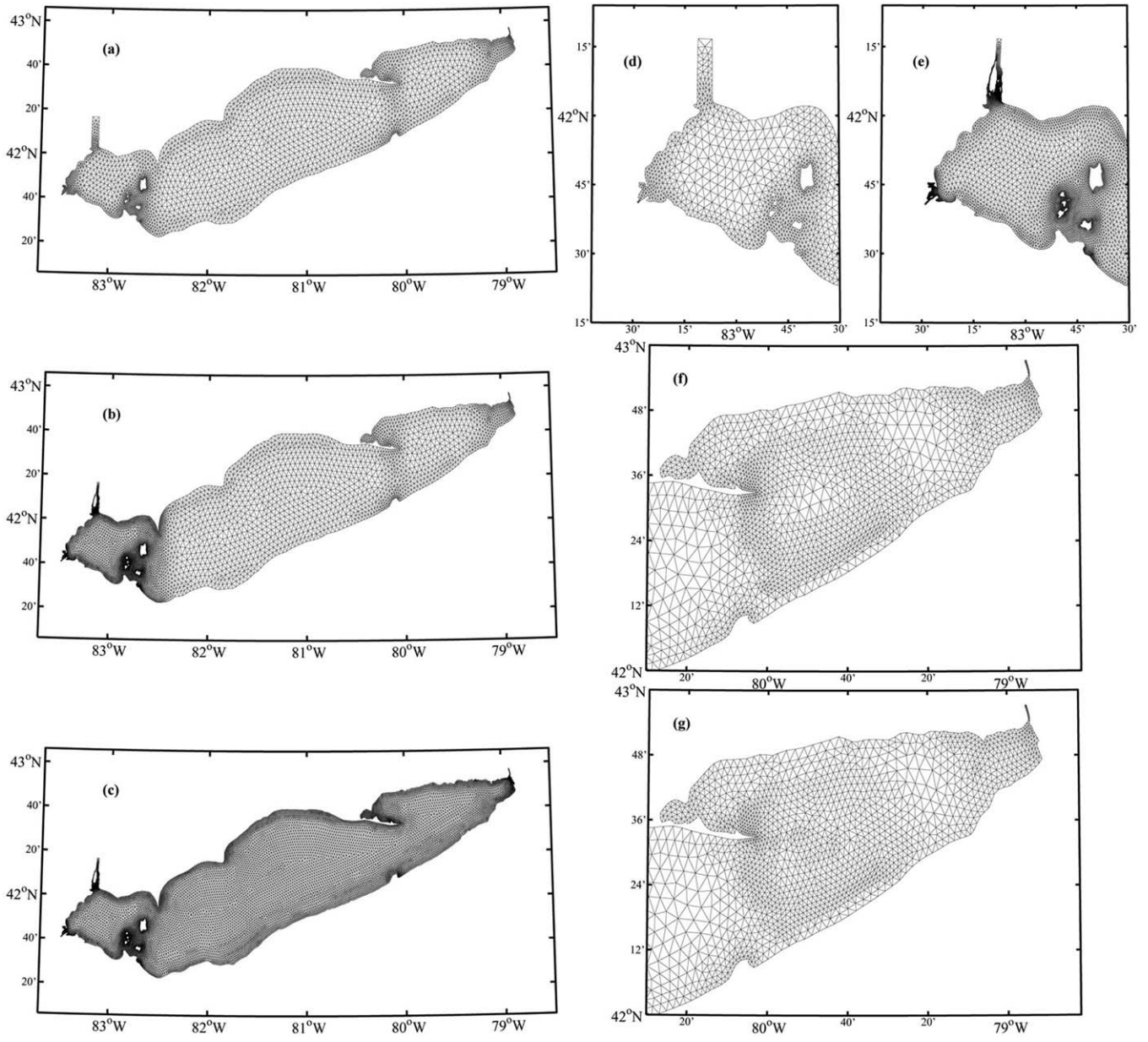

Figure 2. Unstructured grids of the model overlying Lake Erie of (a) Grid V1 (0.25–7.77 km), (b) Grid V2 (0.017–7.77 km) and (c) Grid V3 (0.017–3.69 km), and grids overlying in the WB of (d) Grid V1 and those of (e) Grid V2/V3, and grids overlying the EB of (f) Grid V4 and (g) Grid V5.

The model domain covers the entire lake, including the Detroit and Niagara River channels (Figure 1). Five sets of horizontal grids were used for the model calibration. Grid V1 is a relatively coarse resolution grid (0.25–7.77 km; Figure 2a), and Grid V3 has much finer resolution (0.02–3.69 km; Figure 2c). Grid V2 is a combination of the other two versions, with high-resolution grid in the WB and coarser-resolution grid in the CB and EB (0.02–7.77 km; Figure 2b). Gird V4 and Grid V5 are based on Grid V2, with refined horizontal grids overlying the EB (Figures 2f and 2g).

The bathymetry was derived from the NOAA National Geophysical Data Center U.S. Great Lakes Bathymetry (http://www.ngdc.noaa.gov/mgg/greatlakes/greatlakes.html). The minimum depth was set to be 0.5 m. Based on Courant-Friedrich-Lewy (CFL) criterion, the internal mode time step of the FVCOM integration was 12 s, and the external mode time step was set to be 3 s. Model simulations were initialized on 1 April of each year (1995, 1996, and 2002–2008) respectively, with a uniform water temperature of 3°C, and model runs ended on 30 November each year.

2.2. External Forcing

Three major rivers around the lake were considered in the model (Figure 1). The Detroit River is the major inflow with a mean flux of 5300 $m^3\ s^{-1}$. The Niagara River links Lake Erie to Lake Ontario, and serves as the most important outlet for the lake (5700 $m^3\ s^{-1}$) [*Bolsenga and Herdendorf*, 1993]. Inflow of the Maumee River is much lower than that of the Detroit and Niagara Rivers (136 $m^3\ s^{-1}$). It is the second largest inflow of the lake [*Bolsenga and Herdendorf*, 1993], and has the largest watershed ($\sim$17,000 km^2) of all the tributaries around Lake Erie [*Brant and Herdendorf*, 1972]. In the model, the Niagara River was considered as an open boundary with a specified water elevation, while the Maumee and Detroit Rivers were taken as flow boundaries using specified hourly river flux and water temperature.

Discharge and water temperature of the Maumee River were derived from station 04193500 of United States Geological Survey (USGS). Water temperature of the Detroit River was derived from a regression analysis between historical water temperature of the Detroit River [*Muth et al*., 1986], and air temperature at the surface weather station at Windsor, Ontario (YQG). Discharge of the Detroit River was estimated by an empirical stage-fall-discharge equation [*Fay and Kerslake*, 2009], and a theoretical unsteady flow model developed by *Quinn and Wylie* [1972]. The estimations of hourly river flux during 2009–2012 from both methods were given compared to the corresponding field data from USGS station 04165710 (Fort Wayne, Detroit, MI). The result of the stage-fall-discharge equation has a better performance (correlation coefficient with observational data, $R = 81\%$ versus 70% for the unsteady flow model), and was applied here for the Detroit River discharge. Inflows were distributed equally in the vertical layers because of the shallowness of the river channels (less than 10 m).

The model is forced with hourly air temperature, net downward shortwave radiation (H_{sr}), and upward long-wave radiation (H_l), combined with cloud cover and relative humidity at the lake's surface. These data were provided by NOAA Great Lakes Environmental Research Lab (GLERL). The heat fluxes were processed based on *McCormick and Meadows* [1988], where H_{sr} was calculated based on the in situ latitude and longitude, time of day, day of year and cloud cover, and H_l was calculated using the bulk aerodynamic transfer formulas related to specific humidity of air and water, and surface wind speed. Precipitation and evaporation are not considered in the model, because the net evaporation in Lake Erie is only $\sim$40 $m^3\ s^{-1}$, which is trivial compared to the contribution of surrounding rivers ($\sim$5500 $m^3\ s^{-1}$) [*Neff and Nicholas*, 2005].

Three versions of surface wind forcing ("OB_wnd" "GEM_wnd," and "NARR_wnd") were incorporated into the model. OB_wnd was provided by NOAA GLERL, and is generated based on meteorological stations and buoys within and around Lake Erie. The wind observation data were derived from both NOAA National Data Buoy Center (NDBC) (http://www.ndbc.noaa.gov/), and NOAA National Climate Data Center (NCDC) (http://www.ncdc.noaa.gov/). Similar methods applied in Lake Michigan [*Beletsky and Schwab*, 2001] were used to interpolate wind speed from observations to the computational domain, including an empirical adjustment for the difference between overland and overlake aerodynamic roughness. Because *Beletsky et al*. [2013] found that the GEM_wnd could better reproduce the circulation and thermal structures in the CB of Lake Erie during summer 2005, GEM_wnd was included for the comparison. It was obtained from a regional Global Environmental Multi-scale (GEM) model with 10 km resolution [*Côté et al*., 1998], operated by Environmental Canada Canadian Meteorological Centre. NARR_wnd is at a 3 hourly time interval and with an approximate 32 km horizontal resolution. It was derived from the North America Regional Reanalysis (NARR) model, which is a long-term set of consistent climate data on a regional scale that covers all of North and Central America and much of the flanking ocean regions [*Mesinger et al*., 2006]. Comparisons between the OB_wnd and NARR_wnd in Lake Ontario found no obvious differences [*Wilson et al*., 2013], while the average magnitude of NARR_wnd is much weaker (4.5 m/s) than that of the OB_wnd and GEM_wnd (6.6 and 5.8 m/s) in Lake Erie.

2.3. Observational Data

To evaluate the model's performance in reproducing lake dynamics, the water surface elevation, water temperature, and velocity were calibrated using field data from 2005 (presented in this paper) and validated with data from years 2004 (presented along with results of 2005 in this paper), and 2006–2008 (locations of stations are shown in Figure 1). Water elevation was obtained from eight stations from NOAA CO-OPS (Center for Operational Oceanographic Products and Services). Other variables were compared with field data from IFYLE (International Field Year for Lake Erie; www.ifyle.org), which is managed by NOAA GLERL.

Table 1. Summary of 2005 Model Runs

	Modification of Thermal Scheme		External Forcing		
Case Name	Vertical Thermal Mixing Adjustment	Horizontal Thermal Diffusion Adjustment	Hydraulic flows	Surface Wind Forcing	Surface Heat Flux
Base ($P3_4$ in Table 2)	No	No	Yes	OB_wnd	Regular
C1	Yes	Yes	Yes	OB_wnd	Regular
C2	Yes	Yes	No	OB_wnd	Regular
C3	Yes	Yes	Yes	OB_wnd	No heat flux
C4	Yes	Yes	Yes	No wind forcing	Regular

Simulated thermal and circulation structures were validated with field data from 14 stations. Results presented in this paper are from stations (in situ water depth): S02 (10m), S07 (24.5m), S12 (53.5m), which are moored at the centers of the three basins, respectively (Figure 1). Measurements of current velocities were made via upward-looking 300 kHz RDI acoustic Doppler current profiles mounted 0.5 m above the bottom. Water temperature was measured with Seabird SBE39 temperature loggers. Detailed information of the mooring instruments was illustrated in *Hawley and Eadie* [2007].

2.4. Model Experiments

Based on the calibrated model illustrated in section 3 (case C1), the model was conducted for years 1995, 1996, and 2002–2008 to investigate the interannual variability of hydrodynamics in Lake Erie, because these years were found to have significant variation in yellow perch *Perca flavescens* fishery recruitment. Hydrodynamics in the lake were investigated during different seasons, including spring (April, May, and June), summer (July, August, and September), and early winter (November). To investigate the interbasin water exchanges, we examined the cross-section velocities and the volumetric transports through transects at intersections of the three main basins during 2005 (Figure 1). The transects include the passages north of the Pelee Island (NP), between the Pelee and Kelly Islands (PK), south of Kelly Island (SK), along the Long Point Bridge (ALP), and through the Pennsylvania Channel (PC). To investigate the driving mechanisms in the interannual variability and interbasin exchange dynamics, three additional cases were carried out, which excluded the effect of river inflows (i.e., no flow or open boundaries; case C2), baroclinic processes (case C3), and surface wind forcing (case C4) during 2005 (Table 1), and the results were compared to the result of case C1.

2.5. Model Evaluation

To appraise the model's performance, correlation coefficients (*R*) and root mean square deviation (*RMSD*) for two scalars *x* and *y*, as well as vector correlation coefficients (*VR*) between two vectors $\overrightarrow{W_1}=u_1\vec{i}+v_1\vec{j}$ and $\overrightarrow{W_2}=u_2\vec{i}+v_2\vec{j}$, were applied, given the definition below.

$$R=\frac{\sum_{i=1}^{N}(x_i-\bar{x})(y_i-\bar{y})}{\sqrt{\frac{1}{N}\sum_{i=1}^{N}(x_i-\bar{x})^2}\sqrt{\frac{1}{N}\sum_{i=1}^{N}(y_i-\bar{y})^2}}$$

$$RMSD=\sqrt{\frac{\sum_{i=1}^{N}(x_i-y_i)^2}{N}}$$

Table 2. Summary of 2005 Model Runs for numerical errors in the EB

Case Name	Horizontal Resolution	Vertical Resolution (Uniform Sigma Layers)	Zero HD	Weighting of Vertical Thermal Mixing
P1	Grid V2	20	Yes	No
$P2_1$	Grid V4	20	No	No
$P2_2$	Grid V5	20	No	No
$P3_{1,2,3,4,5,6}$	Grid V2	6, 10, 14, 20, 26, and 30, respectively	No	No
P4	Grid V2	20	No	Yes
P5	Grid V2	20	Yes	Yes

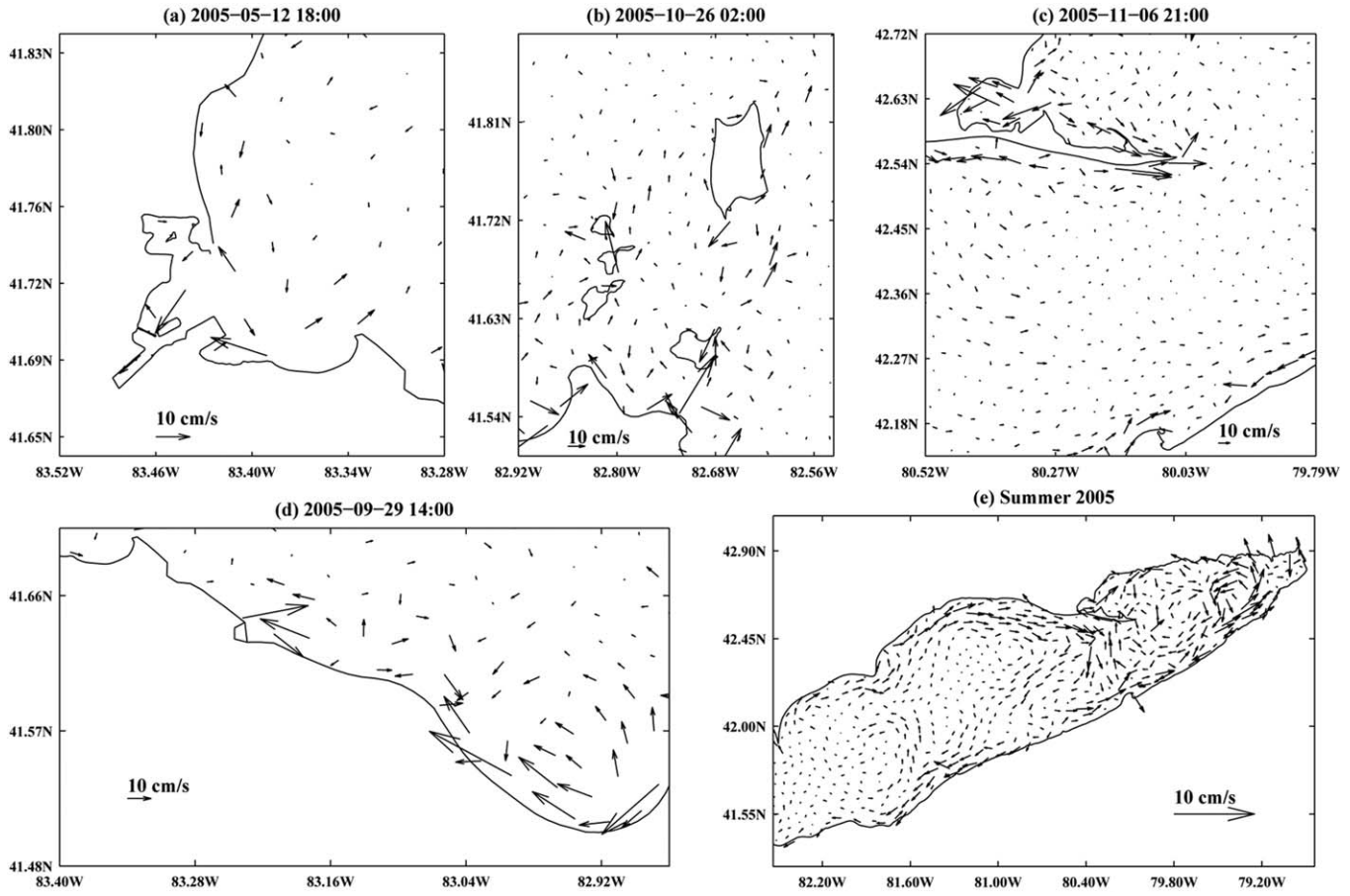

Figure 3. Bias of the depth-averaged circulations between the simulations with Grid V1 and Grid V2 (a, b, d), and Grid V2 and Grid V3 (c, e) in (a) the Maumee River mouth, (b) areas adjacent to Pelee, Bass and Kelly islands, (c) the Long Point Bridge, (d) the southern shore of the WB; and (e) the CB and EB.

$$VR^2 = TR\left(\left(\sum 11\right)^{-1}\sum 12\left(\sum 22\right)^{-1}\sum 21\right)$$

In the definition of VR, $\sum ij = \begin{bmatrix} \sigma(u_i, u_j) & \sigma(u_i, v_j) \\ \sigma(v_i, u_j) & \sigma(v_i, v_j) \end{bmatrix}$, σ is the correlation covariance, and TR is the trace of the products of the $\sum ij$ submatrices [*Crosby et al.*, 1993].

3. Model Calibration

3.1. The Effect of Horizontal and Vertical Grid Resolutions on Lake Dynamics

Simulations were conducted by using three sets of model grids. Choice of model grid had little effect on the water elevation simulation; however, the influence of horizontal grid resolutions on the simulation of lake circulation was significant. During model simulation periods, there was little difference in reproducing midlake circulations with different sets of horizontal grids. However, the model with refined horizontal grids produced stronger nearshore currents during spring and early winter storms (Figures 3a–3d), and stronger gyres in the CB and EB during summer (Figure 3e). In response to stronger gyres simulated by the refined grids, more heat was conserved within the epilimnion with Grid_V3 during summer, deepening the simulated thermocline by ~0.5 m. It should be noted that the differences in the midlake dynamics with different horizontal grids are trivial compared to the differences in the nearshore areas (Figure 3).

Case "base" (Table 1) overestimated hypolimnetic (> 18 m) water temperature at S12 during summer with a *RMSD* of 6.1°C (case $P3_4$ in Figure 4a). This error is possibly related to the pressure gradient [*Haney*, 1991; *Mellor et al.*, 1994, 1998] and the along-sigma artificial horizontal thermal diffusion [*Chen et al.*, 2006]. The increase of

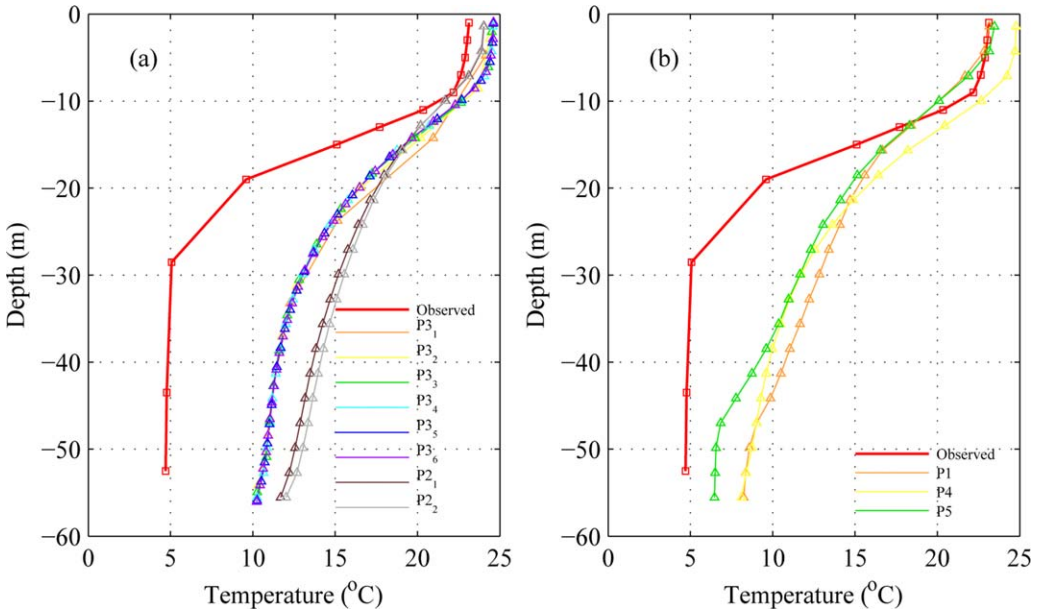

Figure 4. Temperature profiles at S12 during summer 2005: (a) observation and model simulated results of cases with various horizontal and vertical resolutions; (b) observation and model simulated results of cases P1, $P4_4$, P5, and P6.

vertical resolution (case P3 in Table 2) could decrease the error to some extent, while the improvement became insignificant after 20 layers (Figure 4a), which was found in previous studies [*Kliem and Pietrzak*, 1999; *Retana,* 2008]. The increase of horizontal resolution (case P2 in Table 2) led to the growth of the error (Figure 4a) because of density errors [*Mellor et al*., 1994, 1998; *Retana*, 2008]. The combination of zero diffusion [*Mellor et al*., 1998] and weighting ($1+\sigma$ at each layer, where $\sigma=0$ at the surface sigma layer and $\sigma=-1$ at the bottom sigma layer) in the vertical thermal mixing [*Pedersen*, 2010] were suggested to reduce the error. The model's skill in simulating eastward and northward velocities at S12 were improved by 79% and 58%, respectively, and the *RMSD* of simulated hypolimnetic water temperature at S12 was decreased from 6.1°C to 3.2°C (Figure 4b).

Investigations of the influence of horizontal grid resolutions showed the necessity to apply refined horizontal grids in the shallow water areas, and round the river channels. Thus, Grid_V2 was selected as the model's default horizontal grid, because of its sufficient reproduction of dynamics on multiple scales and better computational efficiency compared to Grid_V3. As the model result with the application of 26 or more sigma layers has little improvement over that with 20 sigma layers, 20 sigma layers were selected for model runs.

3.2. The Effect of Various Wind Sources on Lake Dynamics

The GEM_wnd was found to produce more accurate large-scale circulation patterns in Lake Erie during summer, as this wind successfully produced the anticyclonic one-gyre pattern and the bowl-shaped thermocline in the CB during summer of 2005 [*Beletsky et al*., 2013]. Our simulation with the GEM_wnd reproduced similar physical structures in the CB during summer (Figures 5h and 5i), while a two-gyre flow pattern and a tilted thermocline were produced using the OB_wnd (Figures 5e and 5f). The simulation with the NARR_wnd produced a weaker velocity field (Figure 5b) and much shallower thermoclines (Figure 5c). The circulation produced with the NARR_wnd has a two-gyre pattern in the CB, with an anticyclonic gyre in the western part of the basin and an cyclonic gyre in the east of the CB (Figure 5b), which is similar to the climatological summer circulation map produced by *Bai et al*. [2013], in which the NARR_wnd was applied as well. It has the opposite senses of rotation compared to the simulation with the OB_wnd (Figure 5e), observations of *Saylor and Miller* [1987] during 1979–1980, and simulation of GLCFS (Great Lakes Coastal Forecasting System) during 1994 [*Schwab et al*., 2009]. During the model simulation period, the OB_wnd has the best performance in reproducing circulation in the CB, with a *VR* of 68% at S07 compared to those of 53% and 47% of the NARR_wnd and the GEM_wnd.

Compared to the simulated circulations in the WB with wind from the other two sources, the major current produced by the OB_wnd was concentrated in the northern part of the basin during summer (Figure 5e),

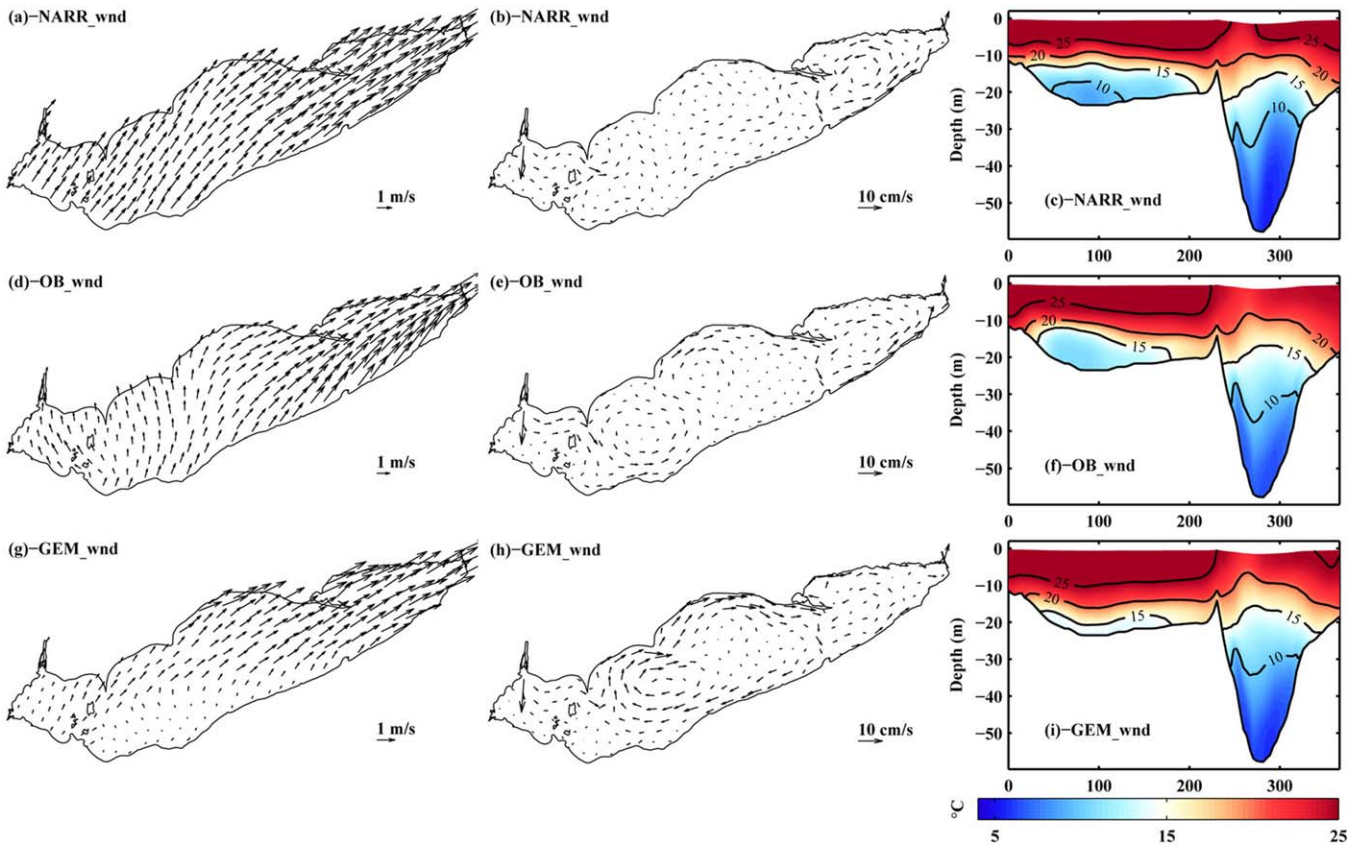

Figure 5. Surface wind forcing (left column), depth-averaged circulations (middle column), and water temperature at the transect ECB (right column) during summer 2005, excited by the NARR_wnd (a, b, and c), the OB_wnd (d, e and f), and the GEM_wnd (g, h, and i).

and had a better consistency with the field data at S02 (*VR* = 62 % versus 34 % and 49 % of the NARR_wnd and the GEM_wnd). Also, this northward concentrated flow was consistent with the observation in Lake Erie during 1979–1980 [*Saylor and Miller*, 1987]. The performance in reproducing circulation in the WB with different wind sources indicates the substantial role of surface wind forcing in dynamics within the basin. The simulated circulations in the EB were similar among results with different wind specifications, with a better skill for the OB_wnd (*VR*=54% versus 46% and 45% for the NARR_wnd and the GEM_wnd at S12). All of them featured a dominant cyclonic gyre in the basin, with another small anticyclonic gyre in the north (Figures 5b, 5e, and 5h). However, the dominant gyre simulated with the NARR_wnd was stronger and located further north compared to the ones produced by wind from the other two sources. These discrepancies were related to the weaker wind-induced mixing processes excited by the NARR_wnd, which resulted in sharper density gradient (Figure 5c) and thus a stronger gyre pattern.

Aside from the circulation and thermal structures, how wind from various sources affect the water level simulation was compared using field data from eight stations. Benefiting from the reality of the OB_wnd in the nearshore regions, the simulated water elevation with the OB_wnd had the best accordance with the observational data (*R* = 81%; *RMSD* = 0.07 m), while simulations with the NARR_wnd had the worst consistency with observational data (*R* = 55%; *RMSD* = 0.11 m). The results using the GEM_wnd were in between (*R* = 73 %; *RMSD* = 0.09 m).

Overall, the NARR_wnd has the worst performance, and the OB_wnd has the best performance in reproducing lake dynamics. The differences in the performances with the OB_wnd and NARR_wnd slightly differed from conclusion of *Wilson et al*. [2013] in the Lake Ontario, partially because of the scarcity of observed wind stations (12 applied in *Wilson et al*. [2013]) in Lake Ontario compared to those around Lake Erie (∼30 around Lake Erie) [*Schwab and Bedford*, 1994] and the absence of empirical adjustment for the overland and overlake aerodynamic roughness during data interpolation in Lake Ontario [*Wilson et al*., 2013]. Though

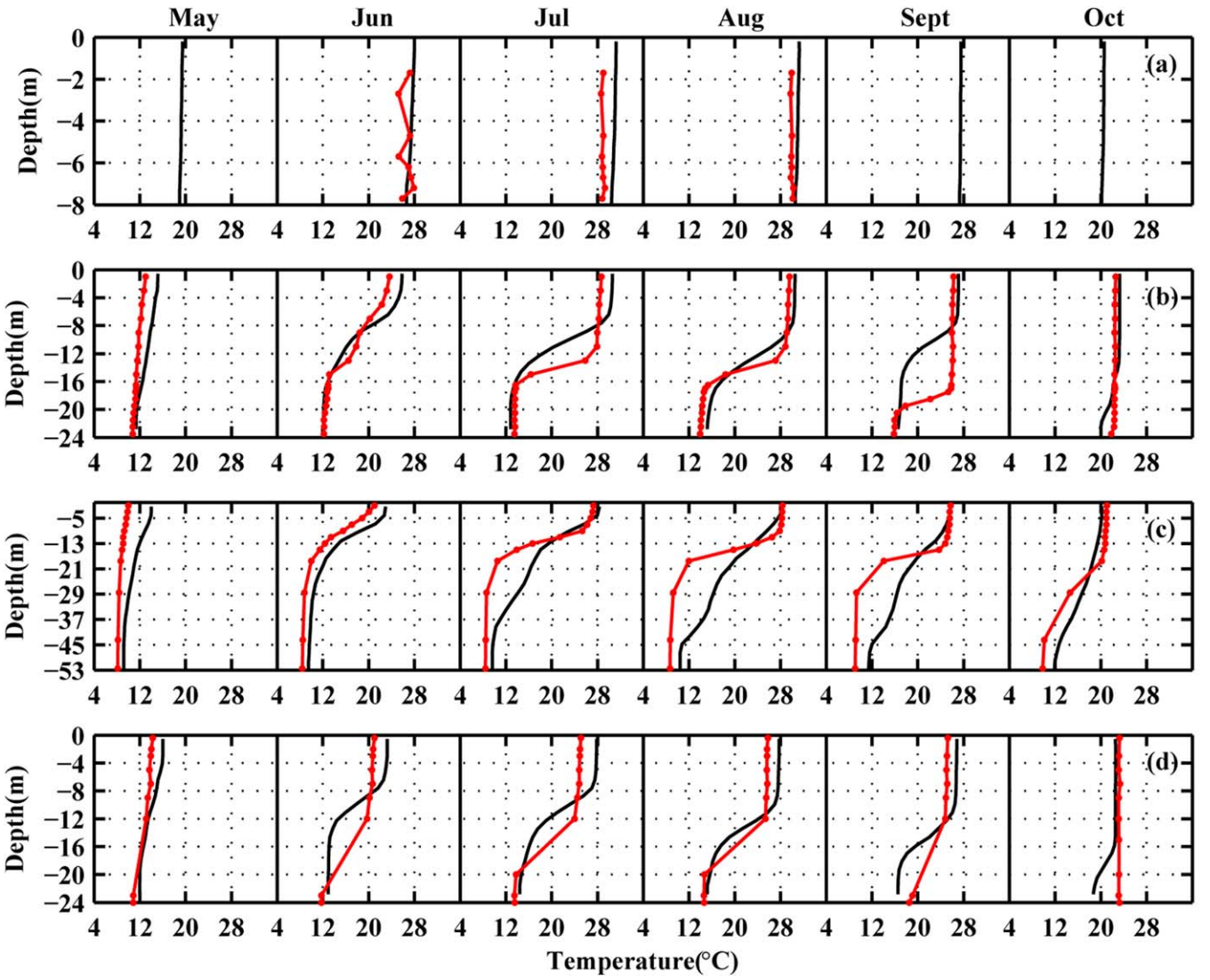

Figure 6. Modeled (black; case C1) versus observed (red) monthly mean temperature profiles at stations S02 (a), S07 (b), and S12(c) during 2005, and station S07 (d) during 2004.

the GEM_wnd could reproduce physical structures in the CB during summer 2005, the overall performance of the OB_wnd still exceeded that of the GEM_wnd in an interseasonal cycle across the whole lake, and it could successfully reproduce physical structures in the CB during summer 2004 (Figures 6d, 7g, and 7h). Further considering the longer availability of the OB_wnd (since 1995) compared to the GEM_wnd (since 2005), the OB_wnd was adopted into the model as the default surface wind forcing.

3.3. Statistical Analysis

The model simulation with Grid V2, 20 sigma layers, and the OB_wnd is compared with field data for model evaluation. Water elevation simulations were quite accurate across the whole lake (eight stations depicted in Figure 1) with *RMSD* ranging from 0.05 to 0.1 m, and a mean *R* of 81 %, which are comparable with the results of GLCFS in Lake Erie [*Beletsky et al*., 2013]. Storm surge events and seiche oscillations were reasonably reproduced, and the underestimation of surge events during extreme storms was related to the smoothness of interpolated wind. Model performance in reproducing circulation and temperature was in good agreement with the observational data as well. The basic thermal structure in the each basin of Lake Erie was satisfactorily reproduced (Figure 6), and the *VR* of the simulation of the velocity with the field data were in the range of 54%–67% (Figure 7), which are comparable to previous applications of FVCOM in other Great Lakes [*Anderson and Schwab*, 2013].

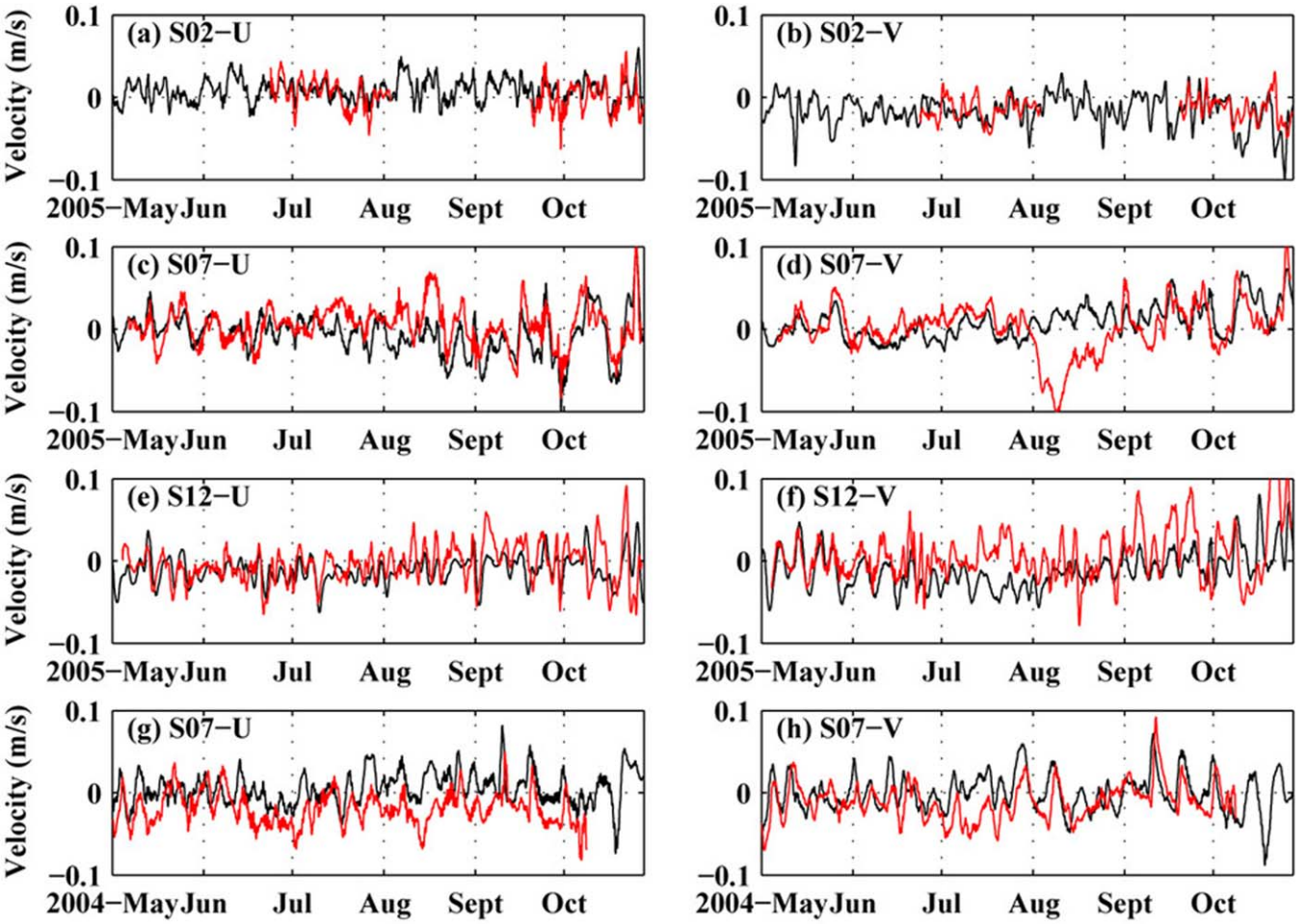

Figure 7. Modeled (black; case C1) versus observed (red) depth-averaged current velocity with 12 h filter at stations S02 (a, b), S07 (c, d), and S12 (e, f), during 2005; and those of S07 (g, h) during 2004.

4. Discussion

4.1. Interbasin Water Exchange and Interannual Variability

4.1.1. Interbasin Water Exchange

The water exchanges between the EB and CB were geographically divided into two systems (Figures 8d and 8e). The eastward transport (C2E) was concentrated in the epilimnion ($<$ 10 m), and the westward transport (E2C) was concentrated in the hypolimnion (Figures 8d and 8e). This conforms to the observations of *Boyce et al*. [1980] during 1977 and those of *Chiocchio* [1981] during 1978. The strongest eastward transport was found in the northern ALP transect (Figure 8d), and the strongest westward transport was found at the bottom of PC transect (Figure 8e). The PC transect area was smaller compared to the ALP (2.2×10^5 m^2 compared to 7.5×10^5 m^2 for ALP) but was deeper (18 m compared to 15 m for ALP). 2673 $m^3 s^{-1}$ out of the total 10097 m^3 s^{-1} C2E transport (26.5 %) was through the transect PC (Figures 9d and 9f). Meanwhile, the majority of the E2C transport was through the transect PC instead of the ALP (57.5 % in a non-ice annual cycle; Figures 9d and 9f). This is consistent with the observation of *Chiocchio* [1981] in 1978, which found that the 80% to 100% of E2C transport was through the PC transect during stratification.

The water exchange from the WB to the CB (W2C) was mainly through the NP transect (75.5%), and some of it was through the southern parts of the PK (19.6%) and SK (4.9%) transects (Figures 8a–8c, 9a–9c). This is consistent with the observation of *Saylor and Miller* [1987] during 1979 to 1980, which found that the water transport through the NP transect is comparable to that from the Detroit River. Meanwhile, the major eastward transport through the NP transect was more concentrated in the top 5 m of the NP transect (2575 m^3 s^{-1} for transport at the surface 5 m, versus 1425 m^3 s^{-1} for

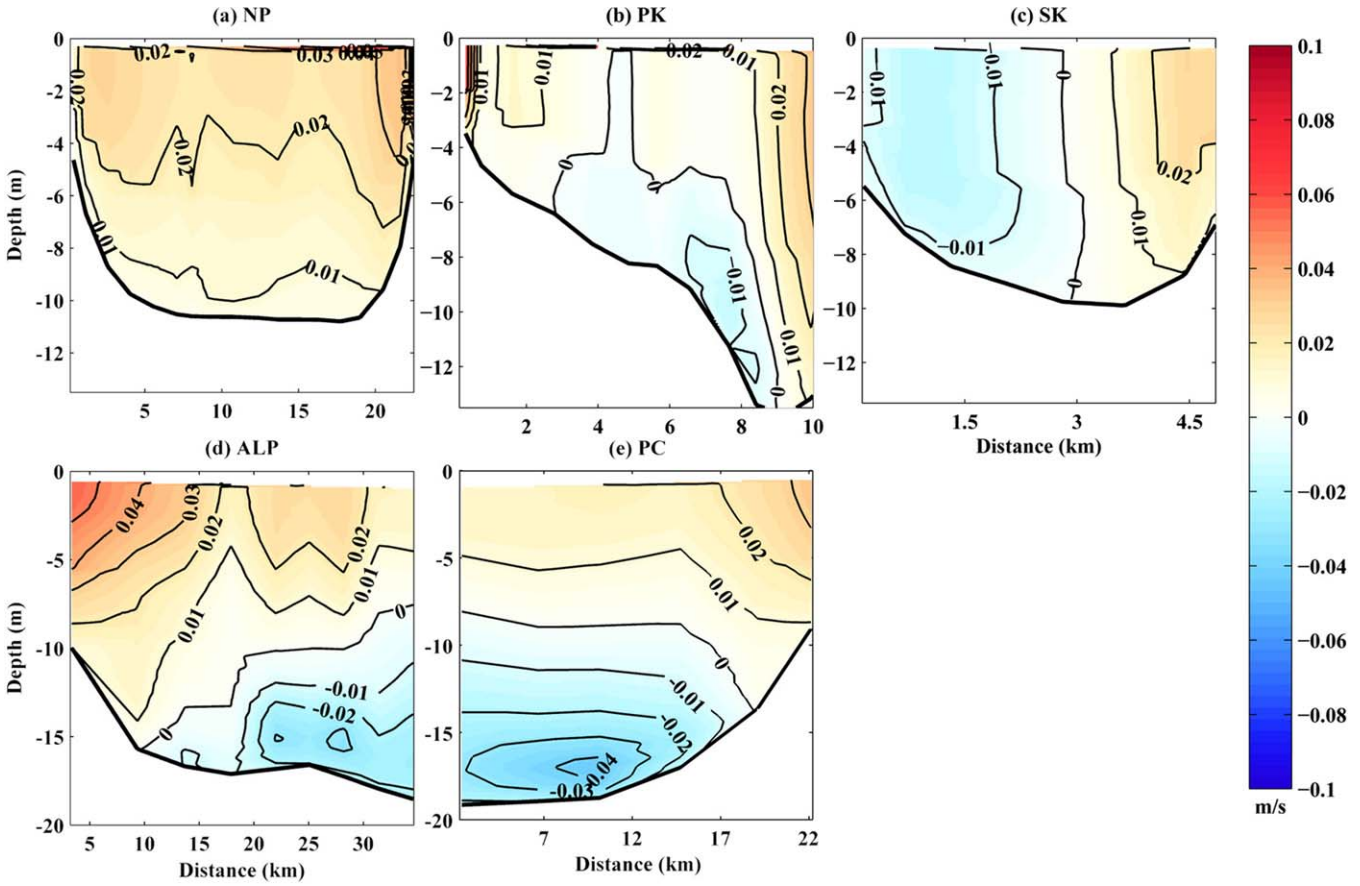

Figure 8. The cross-section velocity (positive toward the east) at transects NP (a), PK (b), SK (c), ALP (d), and PC (e) of case C1 during April–November 2005. Distances of the transects are oriented from the north to the south.

transport below 5 m) (Figure 8a). The water transport from the CB to the WB (C2W) was weaker than that of W2C (415 $m^3\ s^{-1}$ versus 5298 $m^3\ s^{-1}$), and flowed mainly through the bottom of the PK transect (168 $m^3\ s^{-1}$; Figure 8b) and the northern part of the SK transect (247 $m^3\ s^{-1}$; Figure 8c). Little C2W transport through the NP transect was detected during model simulation period (Figure 8a), which is consistent with the conjecture of *Bartish* [1987]. During the simulation years, relatively significant C2W through the NP transect was only found during years 2006 and 2008, and they were still trivial (0.06 $m^3\ s^{-1}$ and 81 $m^3\ s^{-1}$) compared to those through the SK and PK transects (330 $m^3\ s^{-1}$ and 185 $m^3\ s^{-1}$). These unusual C2W transports through the NP transect were likely related to the intrusion of hypolimnetic water from CB to WB through the NP transect during summer. This "cold-tongue" intrusion from the CB has been observed during August 1980 [*Bartish*, 1984].

4.1.2. Interannual Variability

Lake surface temperature (LST) is an important component of the coupled lake-atmosphere system and its anomalies fluctuated in the range of±1.2°C for all the simulated years (Figure 10). Warm phases appeared during years of 2002, 2004, 2005, and 2007, and cold phases appeared during other simulation years. In particular, LSTa was extremely high during 2005 (Figure 10f), and an extreme cold phase occurred in 1996 (Figure 10b). It should be noted that the LSTa was not spatially homogeneous across the whole lake, and reverse phase patterns were found in the CB during 2004 and 2006. Warm and cold bands of LSTa alongshore in the CB and EB were detected during most of the simulation years, and a cold-water mass also appeared at the river mouth of the Detroit River during 2004 (Figure 10).

Through these 9 years of model simulation, little interannual variability of the dynamics in the EB was found, which illustrates that it is a typical example of lake-induced mesoscale circulation systems superimposed on the regional meteorological flow. Some interannual variability was detected for

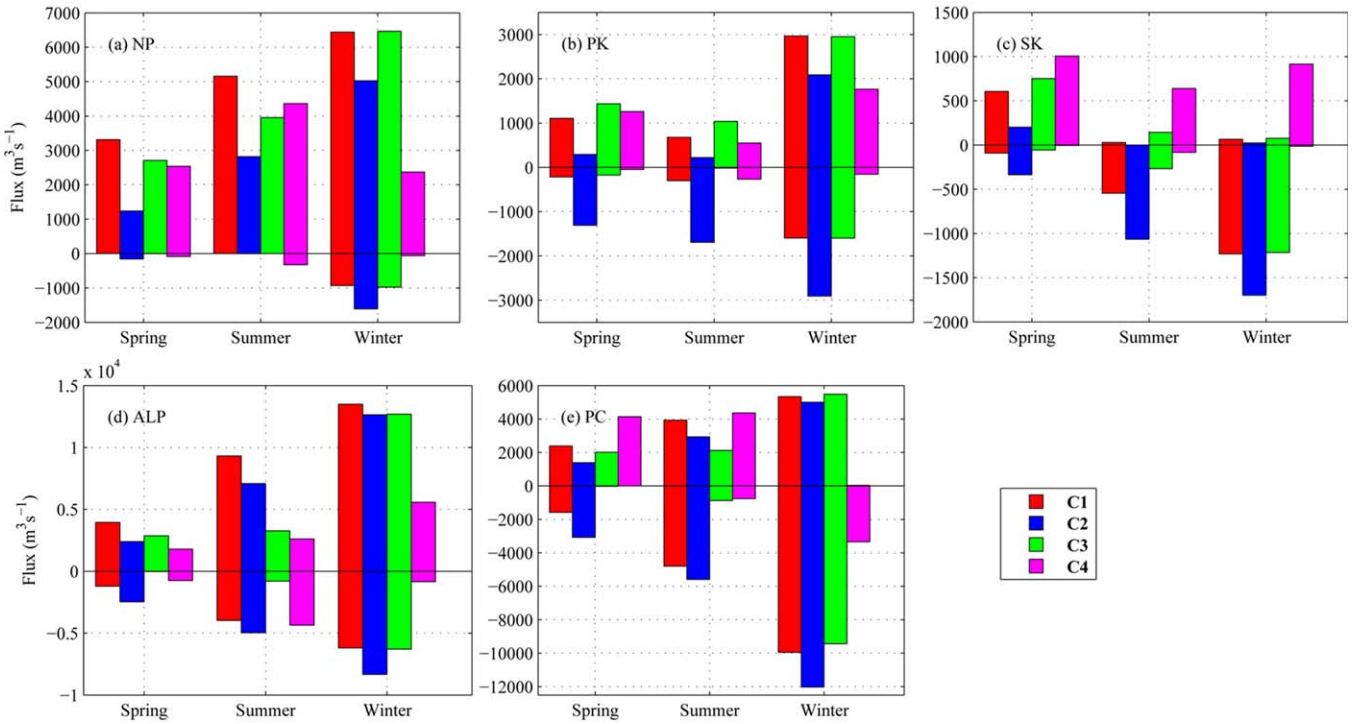

Figure 9. The eastward (positive) and westward (negative) interbasin volumetric transports at transects NP (a), PK (b), SK (c), ALP (d), and PC (e) of cases C1, C2, C3, and C4.

hydrodynamics in the WB. Dynamics in the CB, especially during summer, varied significantly year by year. A similar phenomenon was found in the southern basin of Lake Michigan as well, where the circulation in the basin varied significantly during different model simulation years [*Beletsky and Schwab*, 2001]. Three typical summer physical structures in the CB were identified (Figure 11). During 1995, a strong cyclonic gyre predominated circulation in the basin, resulting in a dome-shaped thermocline

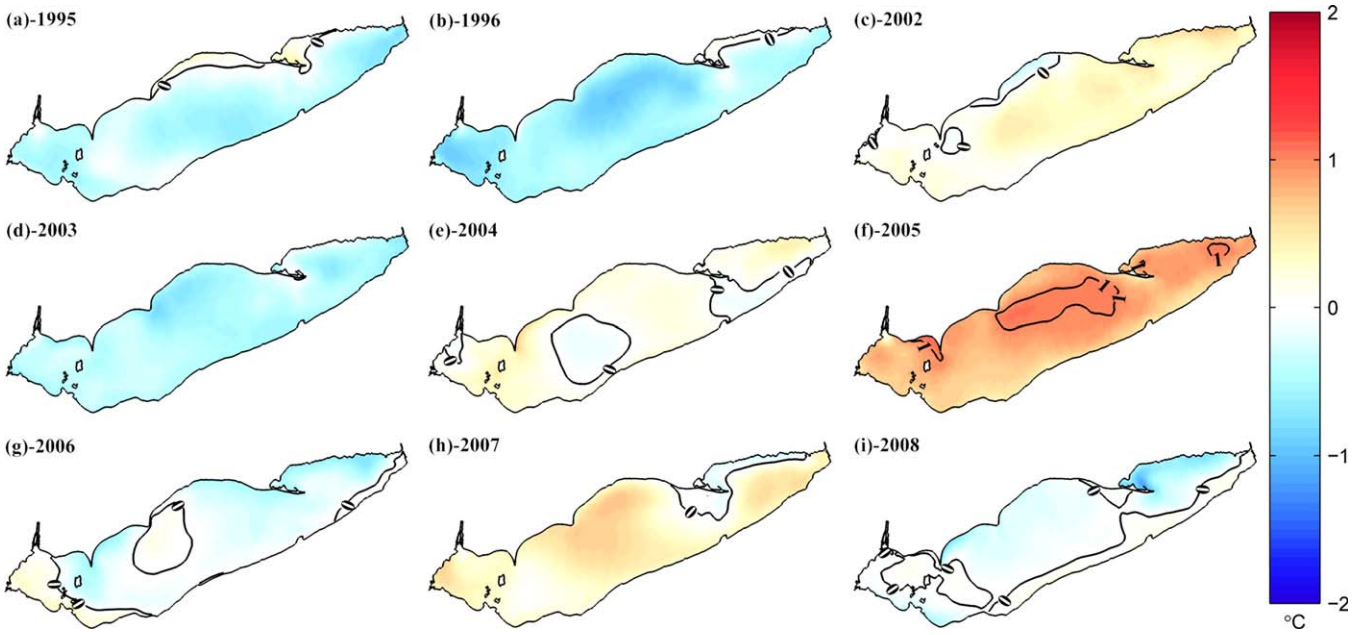

Figure 10. LSTa (April–November) during 1995, 1996, and 2002–2008.

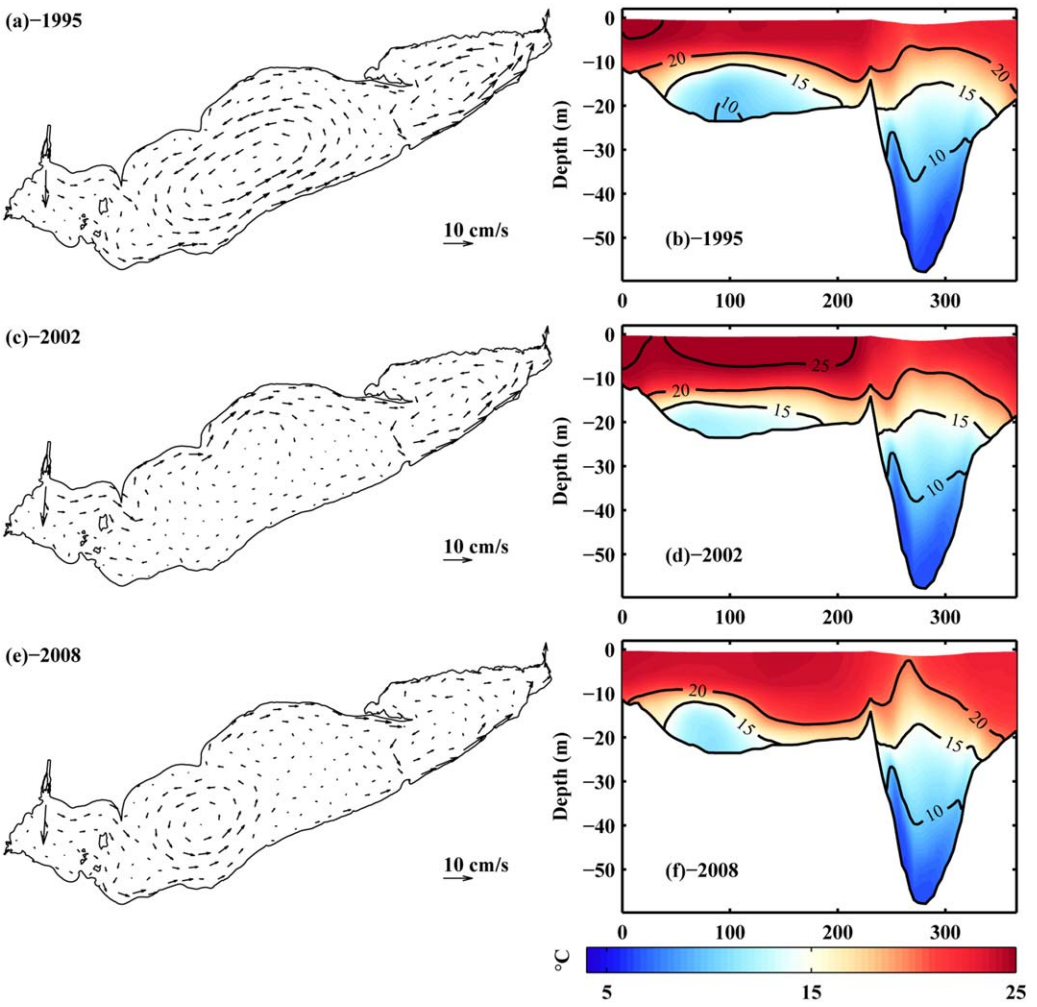

Figure 11. The depth-averaged circulation and water temperature at the transect ECB during summer of 1995 (a, b), 2002 (c, d) and 2008 (e, f).

and a shallow epilimnion (Figures 11a and 11b). In years 2002 and 2003, a weak, anticyclonic gyre formed in the basin, leading to a "flat" thermocline parallel to the lake's bottom (Figures 11c and 11d). Typical two-gyre circulation patterns, with a dominant cyclonic gyre and tilted thermocline, appeared in 2004, 2006, and 2008 (Figures 11e and 11f). Similar two-gyre patterns with a stronger anticyclonic gyre were simulated during years 2005 and 2007, in contrast to the findings of *Beletsky et al*. [2012] where circulation in the CB was dominated by a strong anticyclonic gyre during these 2 years. The larger interannual variability of dynamics in the CB were likely to be driven by the variation of the surface wind stress curl ($\frac{\partial \tau_y}{\partial x} - \frac{\partial \tau_x}{\partial y}$, where τ_x and τ_y are wind stress along the x and y directions, respectively), which was proved to be the driving mechanism for circulation in the CB [*Beletsky et al*., 2013].

The depth-averaged spring circulation over 9 years features strong hydraulic flows in the WB, and cyclonic gyres in the CB and EB (Figure 12a), which is similar to the simulation of surface currents with GLCFS (http://www.glerl.noaa.gov/res/glcfs/). The depth-averaged summer circulation pattern over 9 years is illustrated in Figure 12b. Compared to the simulation of *Bai et al*. [2013], a stronger eastward flow along the northern shore was reproduced, which was observed during summer 1979–1980 [*Beletsky et al*., 1999] (Figure 12d). A cyclonic circulation was found in the EB, which is consistent with previous findings [*León et al*., 2005; *Bai et al*., 2013; *Beletsky et al*., 2013]. The streamlines of the flow field formed two counter-rotating closed gyres in the CB, with a dominant cyclonic gyre at the southwest and a weaker anticyclonic one near the northeast of the basin. The simulated gyres in the CB

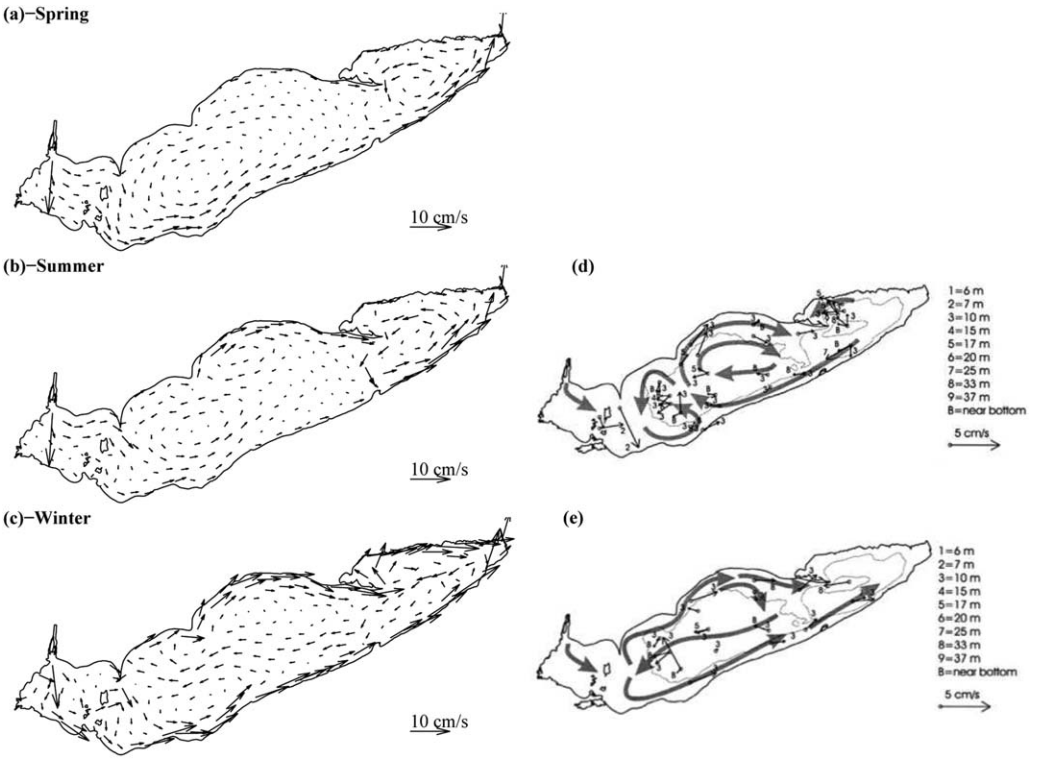

Figure 12. Modeled long-term depth-averaged circulation during spring (a), summer (b) and winter (c), and observed depth averaged circulation during summer (d) and winter (e) 1979–1980 [from *Beletsky et al*., 1999].

with our model were of opposite senses compared to the result of *Bai et al*. [2013], but were similar to the observed circulation during summer 1979–1980 (Figure 12d) [*Beletsky et al*., 1999]. The differences in the strength of the simulated gyres in the CB between our model and the observed gyre strength were likely caused by the lack of wind stress curl in the OB_wnd. Factors that may contribute to discrepancies between simulations of our model and that of *Bai et al*. [2013] include the different wind specifications (NARR_wnd applied in *Bai et al*. [2013]) and different time span (1993–2008 for the result of *Bai et al*. [2013]).

In early winter, strong northeastward currents characterized nearshore circulations, corresponding to the prevailing winter winds. A reverse southwestward flow dominated circulation inside the lake (Figure 12c), with a suppressed cyclonic gyre located in the north and another anticyclonic one in the south CB. The inflow of the Detroit River was less dominant in the WB compared to its significance during summer, and circulation in the WB was dominated by strong nearshore currents and southward flow in the basin. The simulated early winter climatological circulation in the lake was similar in structure to the observation during winter 1979–1980 (Figure 12e) [*Beletsky et al*., 1999]. Compared to the result of *Bai et al*. [2013], stronger longshore currents were captured with our model, resulting from refined horizontal grid resolution in the nearshore areas in our model (~0.2 km versus 3.5 km in *Bai et al*. [2013]) and stronger wind forcing of the OB_wnd compared to that of the NARR_wnd applied in *Bai et al*. [2013]. According to our model results, the cyclonic gyre in the EB was deconstructed by the reverse flow during winter, with two small gyres locating at each side of the dominant flow (Figure 12c), while the major cyclonic gyre still existed in the winter circulation map reproduced by *Bai et al*. [2013].

4.2. The Effect of Hydraulic Flows on Lake Dynamics

Based on previous work [*Bartish*, 1987; *Saylor and Miller*, 1987] and our model results, hydraulic flows should be critical to the water exchange between WB and CB, and some further analysis is given here. In response to the prevailing southwesterly wind, circulation induced by hydraulic flows in the WB is concentrated in the northern part of the basin, flowing to the CB through the passage NP

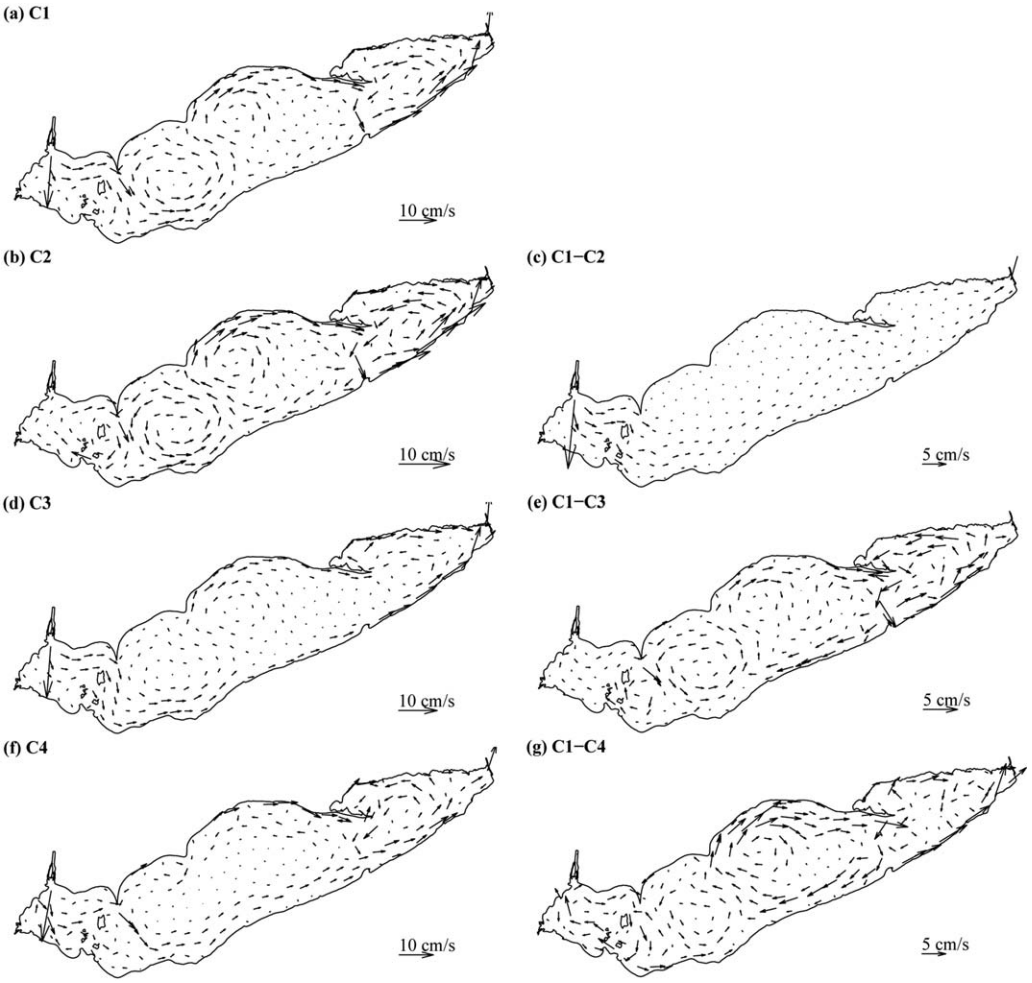

Figure 13. Modeled depth-averaged circulations during spring 2005 of cases C1–C4 (a, b, d, and f), and their bias with the result of case C1 (c, e, and g).

(Figures 13c and 14c). Overall, hydraulic flows have more significant effect on dynamics in the WB during spring and summer (Figures 13c and 14c) than in the winter (Figure 15c), which is related to the difference in magnitude of surface wind forcing. During spring and summer, the weak surface wind forcing (5.7 m/s) was not strong enough to stir the water in the WB, and circulation in the basin was mostly driven by the hydraulic flows (Figures 13b and 14b). Under the strong wind forcing during early winter (9.3 m/s), the circulation in the WB was dominated by an anticyclonic gyre for results of both cases C1 and C2 (Figures 15a and 15b), indicating the dominance of wind-driven currents over hydraulic flows in the basin during early winter. Though the incorporation of hydraulic flows did not modify the basic flow patterns in the CB and EB, they induced an eastward flow in the CB along its southern shore and a northeastward flow in the EB around the Niagara River mouth (Figures 13c, 14c, and 15c). The current from the CB to the EB induced by hydraulic flows was mostly through the PC, and it flowed out of the lake through the Niagara River channel (Figures 13c, 14c, and 15c).

Accordingly, hydraulic flows are of great importance to interbasin water exchanges. They accelerate the eastward transport in the lake, especially for the flows of W2C (Figure 9). When assuming the lake was a closed system (case C2), the total W2C transport was reduced by 57% (Figures 9a–9c). Its influence on the total C2E transport was smaller but still significant (reduced by 29 %; Figures 9d and 9e). The influences of hydraulic flows on the eastward interbasin transports were mainly on transects NP and ALP (Figures 9a and 9d), which accounted for 70% and 68% of the total W2C and C2E

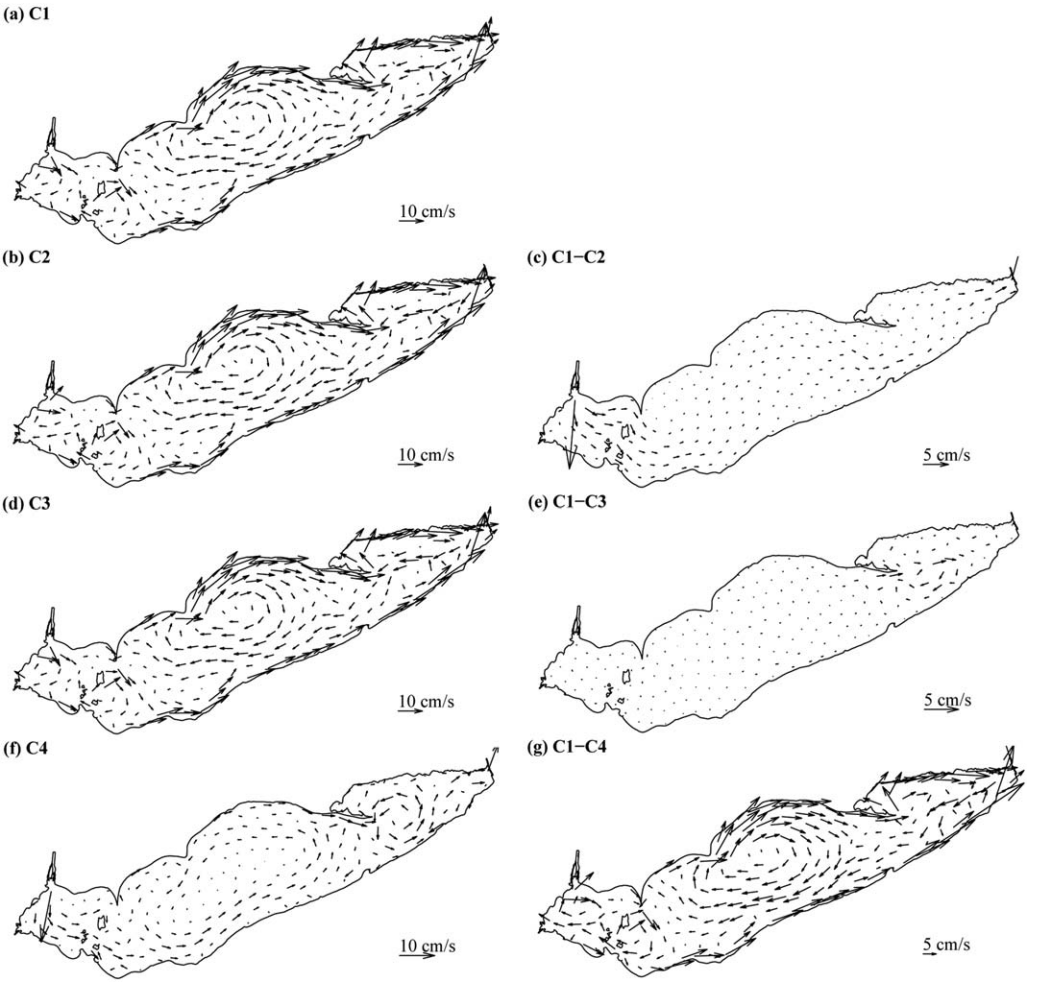

Figure 14. Modeled depth-averaged circulations during summer 2005 of cases C1–C4 (a, b, d, and f), and their bias with the result of case C1 (c, e, and g).

transports induced by hydraulic flows, respectively, and were more significant during spring and summer than during winter. Also, the decrease of the eastward transports mainly occurred on the top layers of the transects, which is expected as river flows flush the whole lake through the epilimnion [*Bartish*, 1987]. Meanwhile, with significant inflow from the Detroit River and outflow through the Niagara River, westward transports in the lake were decreased. When the river flushing through the lake was excluded (case C2), the E2C and C2W transports, especially through the deeper parts of transects NP and PC (Figures 9a and 9e), were increased by 416% and 42%, respectively. This validated the conjecture of *Bartish* [1987] about the significance of hydraulic flows in the low C2W transport rate.

Overall, the hydraulic flows dominate the WB dynamics most of the year (except for the early winter). Thus, the small interannual variability in the riverine water temperature (5% for the Detroit River and 3% for the Maumee River) and discharges (5% for the Detroit River and 23% for the Maumee River) was responsible for the limited interannual variability in physical conditions in WB found in section 4.1.2. Note that though discharge of the Maumee River has a high interannual variability during simulation years, its standard deviation is only 41 $m^3\ s^{-1}$, which is trivial compared to the average inflow of the Detroit River (5300 $m^3\ s^{-1}$). And the momentum contribution of the Maumee River could hardly be detected in a seasonal cycle (Figures 13c, 14c, and 15c). Also, the small variation in water temperature of the Detroit River (0.6°C) was not responsible for the cold-water mass at the Detroit River mouth during 2004 (Figure 10e). When the differences in riverine water temperature with the

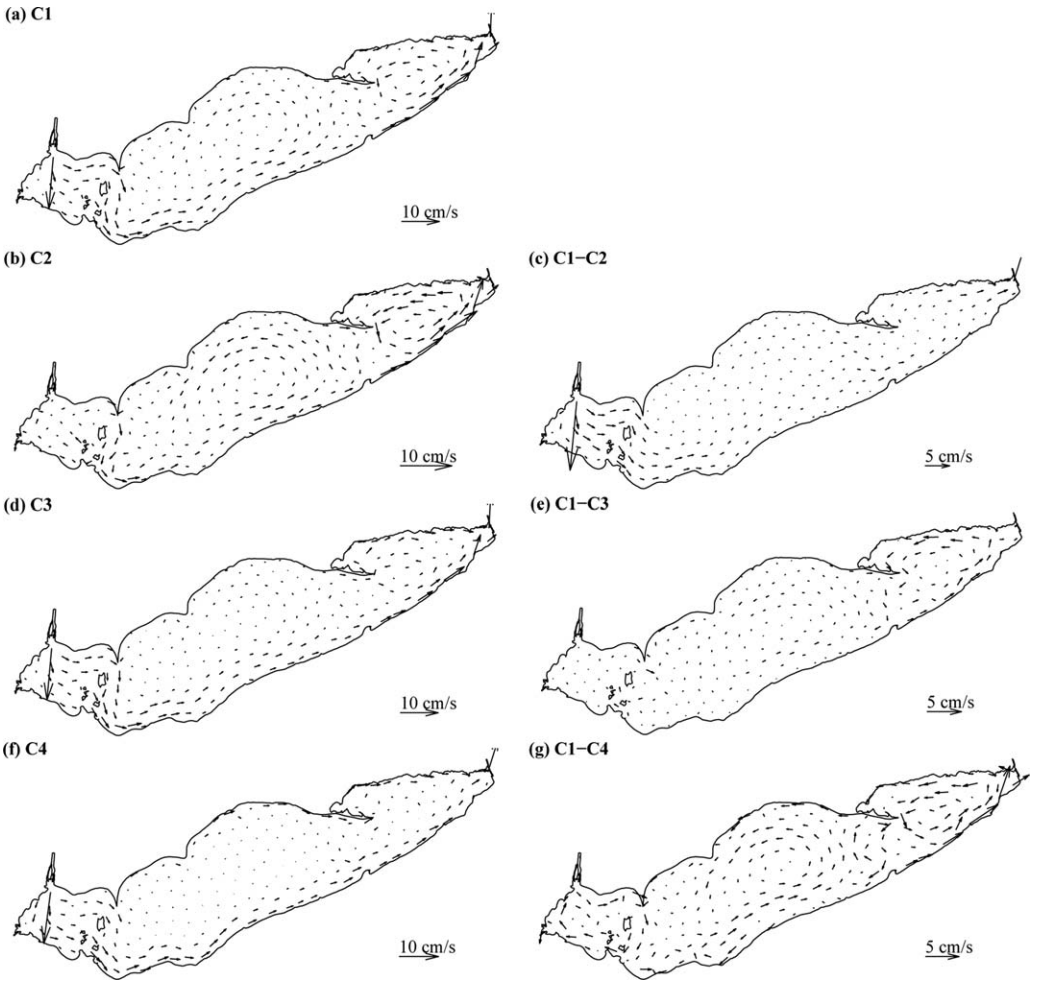

Figure 15. Modeled depth-averaged circulations during winter 2005 of cases C1–C4 (a, b, d, and f), and their bias with the result of case C1 (c, e, and g).

lake water temperature were excluded, this cold tongue still existed. It more likely resulted from the variation in atmospheric forcing.

4.3. The Effect of Atmospheric Forcing on Lake Dynamics

Given the importance of the atmospheric forcing, its effects on lake dynamics were further investigated. The surface heat flux and wind forcing are the two major external forcing functions on the lake. The baroclinic processes induced by temperature gradient had little influence on the lake's spring and winter circulation (Figures 13e and 15e), as most parts of the lake were well mixed during spring and returned to the isothermal state after the overturning during autumn [*Schertzer et al*., 1987]. The bias between the simulated spring and early winter circulations with cases C1 and C3 only existed in the EB (Figures 13e and 15e). This resulted from the early stratification and lag of the overturning processes in the EB in the two seasons, respectively, due to the deepness of the EB. With the incoming heat flux at the lake's surface during spring, full stratification would occur in the CB and EB during summer [*Schertzer et al*., 1987]. When the surface heat flux was excluded (case C3), the cyclonic gyre in the EB during spring and summer was mostly deformed (Figures 13d and 14d), indicating its baroclinic nature. The modeled climatological winter circulation showed deformation of the cyclonic gyre in the EB (Figure 12c) compared to the result of *Bai et al*. [2013]. According to observations at S12, the EB remained isothermal during the winter 2004–2005 (a relatively mild winter with winter gusts of 7.8 m/s). Thus, the destabilization of the cyclonic gyre in the EB during winter is reasonable. The basic summer circulation pattern in the CB was not greatly modified by the exclusion of

baroclinic processes (case C3), but the vorticity of the simulated gyres was weakened by ~60% (Figure 14e). Meanwhile, the baroclinic processes generated a westward flow (~1 cm/s) from the CB to the WB through the transects PK and SK, and another eastward flow (~4 cm/s) from the WB to the CB through the transect NP during summer (Figure 14e).

When the surface wind forcing was excluded (case C4), the pathway of the hydraulic flows in the WB was modified during spring and summer. Instead of flowing along the northern shore as was observed [*Saylor and Miller*, 1987], it spread into the southern WB with weaker strength (Figures 13f and 14f). The summer circulation in the EB was still dominated by a cyclonic gyre in the result of case C4 (Figure 14f). Compared to the result of case C1, the strength of the gyre was slightly magnified when surface wind forcing was excluded (Figure 14g), resulting from the increased pressure gradient with the absence of wind-induced mixing. During spring, the cyclonic gyre in the EB was slightly weakened with the exclusion of surface wind forcing (Figure 13f), which indicates the contribution of the surface wind forcing in generating the cyclonic gyre in the EB during spring. In the result of case C4, the cyclonic circulation in the CB was greatly decreased compared to that of case C1 during spring (Figure 13g), and summer circulation in the CB was dominated by a cyclonic gyre across the basin (Figure 14f) instead of the two-gyre circulation pattern in the result of case C1 (Figure 14a). This is consistent with the conclusions of *Beletsky et al*. [2013] concerning the role of wind stress curl in generating the anticyclonic gyre in the CB during summer. Due to the exclusion of surface wind during the lake's overturning processes, CB and EB remained stratified in the early winter, and cyclonic gyres dominated circulations in the basins (Figure 15f). With the significantly weakened northeastward nearshore current (Figure 15f), and the failure to bring the lake back to the isothermal status, the southwestward reverse flow at the center of the CB and EB was not found in the result of case C4 during early winter (Figure 15f). Also, through its contribution to the lake's heat budget, by excluding the surface wind, the LST increased by 5°C in a non-ice annual cycle. Meanwhile, when surface wind forcing was excluded, the upwelling and downwelling regions shrunk by 34% and 37%, respectively, and the magnitude of upwelling and downwelling was slightly weakened by 4% and 2%, respectively.

Considering the dominant role of wind and heat flux in the density-driven flow, how the density-driven flows influence interbasin water exchanges are discussed to understand the role of atmospheric forcing in the lake dynamics. By assuming the whole lake was thermally homogeneous (case C3), C2E and E2C were reduced by 41% and 78%, respectively (Figures 9d and 9e), especially for the transport through the ALP (Figure 9d) and those during summer. This mechanism was significant for the transport of C2W as well (reduced by 63%), while it had limited effect (7% reduction) on the W2C transport (Figures 9a–9c). The influences of surface wind forcing on the water exchanges through NP (Figure 9a), C2W through PK (Figure 9b), C2E through ALP (Figure 9d), and E2C through PC (Figure 9e) during summer were similar to that of the surface heat flux. It is likely that the surface wind forcing influenced these processes through its contribution to the thermal mixing. Besides, the wind-induced circulation magnified the water exchange through NP, PK, ALP, and PC significantly during winter (Figures 9a, 9b, 9d, and 9e). Additionally, though *Saylor and Miller* [1987] thought that wind plays a minor role in the water exchange between the WB and CB, we found that the surface wind forcing modifies the pathway of the hydraulic flows in the WB. When the surface wind forcing was excluded (case C4), though the total transport of W2C remained similar with that of case C1 (4994 $m^3\ s^{-1}$ versus 5298 $m^3\ s^{-1}$), transport through SK (Figure 9c) significantly increased (63%), with the decrease (19%) of transport through NP (Figure 9a). Subsequently, the transport of C2W through NP and PK was increased from 0 $m^3\ s^{-1}$ to 81 $m^3\ s^{-1}$ (Figure 9a), and that through SK was reduced by 97% (Figure 9c). Thus, the preference of W2C transport through the NP transect recognized by *Bartish* [1987] resulted from the combined effect of hydraulic flows and wind forcing.

Interannual variability in cold and warm phases in LSTa of the whole Lake Erie were determined mainly by the net heat flux at the lake's surface. The overall cold/warm phases match the fluctuation of air temperature recorded by meteorological buoys in the lake, which represented a periodic fluctuation of 3–6 years in a 37 year cycle (1980–2007). Response of LSTa to climate modes cannot be determined due to the limited time span of this study. Considering the significant role of surface wind forcing in generating gyres in the CB (Figures 13g and 14g), the reverse phase patterns of LSTa in the CB during 2004 and 2006 (Figures 10e and 10g) revealed another potential mechanism that regulates LSTa: the vertical flux of cool water into the

epilimnion. This is due to variation in Ekman pumping, and thus to the anomalies of the wind stress curl. The response also indicated the increasing control of wind, rather than the fluctuation of solar radiation in the interannual variability of LSTa in the middle CB. With the contribution of surface wind forcing to the upwelling and downwelling events in the nearshore areas, the warm and cold longshore bands of LSTa in the CB and EB (Figure 10) were thus related to the shift of direction and magnitude of wind forcing. For example, weaker upwelling led to the warm bands on the northern shore during 1995 and 1996 (Figures 10a and 10b), while stronger upwelling events during 2002 and 2007 cooled the surface water at the northern shore (Figures 10c and 10h). Similarly, the warm band during 2008 (Figure 11i) and cold band during 2004 (Figure 10e) at the southern shore were associated with stronger and weaker downwelling events, respectively.

5. Conclusions

The hydrodynamics in Lake Erie were examined on interannual and interseasonal timescales, and interbasin space scales, using an unstructured-grid numerical model or FVCOM. The model was calibrated for horizontal and vertical grid resolutions, and wind from different sources, and showed its capability to produce hydrodynamics within the lake. Dynamics of interbasin water exchange and interannual variability in the lake's circulation and thermal structures were investigated, and the climatological seasonal circulation maps were presented and compared with previous observation and model results. The lake's sensitivity to major external forcing, including hydraulic flows and atmospheric forcing, was examined, and key mechanisms for the interbasin water exchange and the interannual variability were specified. The main conclusions are as follows:

1. River-induced hydraulic flows are of great importance for circulation in the WB, and transport from the CB to EB through the Pennsylvania channel. Hydraulic flow has more influence on dynamics in the WB during spring and summer, whereas it could be overwhelmed by wind-driven circulation during winter storms. Little interannual variability was found for the properties of river inflows around the WB, which is consistent with the limited interannual variability in dynamics in the WB. Surface wind forcing dominates the gyre patterns in the CB, altering the strength of the upwelling and downwelling events, and modifying the pathway of hydraulic flows in the WB. Baroclinic processes are the major mechanism for producing the cyclonic gyre in the EB during spring and summer. Baroclinic processes contributed little in determining the circulation patterns in the WB and CB, while the magnitude of the gyres in the CB and transport between the CB and WB were magnified with the incorporation of baroclinic processes.
2. Water exchange between the WB and CB is mainly eastward (W2C) through the transect NP, which is a combined effect of hydraulic flows and surface wind forcing. The C2W transport, as well as the eastward and westward transports between the CB and EB, is mainly controlled by density-driven flows, which are determined by collective effect of surface heat and wind forcing. The C2E and E2C are comparable with each other with the exclusion of hydraulic flows, and are of greater magnitude compared to the transports between the WB and CB. The westward transports in the whole lake (E2C and C2W) are impeded by the eastward flow induced by the hydraulic flows. Wind-driven circulations magnify the interbasin water exchange during winter.
3. Interannual variability in the lake's general dynamics was mainly found in the CB, and three typical summer physical structures were detected during the simulation years. The interannual variability of LST was in the range of $\pm$ 1.2°C, resulting from the variation of the net heat flux at the lake's surface. Reverse phase patterns were found at the center of the CB, and at the nearshore regions in the CB and EB, which is due to the variation in surface wind forcing. The climatological seasonal circulation maps were presented. In spring, circulation in the WB was dominated by strong hydraulic flows, and those in the CB and EB were dominated by cyclonic gyres. In summer, circulation in the WB was dominated by the hydraulic flows at the northern shore; that in the CB was dominated by circulation with a two-gyre pattern; and that in the EB was dominated by a cyclonic gyre along the depth contours. In winter, the cyclonic gyre in the EB was destabilized, and strong northeastward currents prevailed in the nearshore areas, with a dominant southwestward reverse flow in the center of the lake.

The work conducted here will be useful for other similar lake systems, such as Lake Ontario and Lake Michigan, and it will provide insight for other coastal systems, such as Tampa Bay and Chesapeake Bay.

Acknowledgments
This project is funded by the Great Lakes Fishery Commission. Research was carried on NSF Stampede (Support to M. Xia). NARR Reanalysis data were provided by NCEP/NWS/NOAA/U.S. Department of Commerce (2005), NCEP North American Regional Reanalysis (NARR), from website at http://rda.ucar.edu/datasets/ ds608.0/. Research Data are archived at the National Center for Atmospheric Research, Computational and Information Systems Laboratory, Boulder, Colorado. Long Jiang, a Ph.D student of Xia helped calibrate the model and his effort is appreciated. GEM data were provided by Environment Canada and Dmitry Beletsky from University of Michigan, Ann Arbor. Comments from Kevin Pangle and Jose Marin Jarrin are appreciated. The authors also thank reviewers for their comments. We appreciate additional ADCP data provided by Rao Yerubandi from Environmental Canada. This is GLERL contribution 1749.

References

Anderson, E. J., and D. J. Schwab (2013), Predicting the oscillating bi-directional exchange flow in the Straits of Mackinac, *J. Great Lakes Res.*, *39*(4), 663–671, doi:10.1016/j.jglr.2013.09.001.

Anderson, E. J., D. J. Schwab, and G. A. Lang (2010), Real-time hydraulic and hydrodynamic model of the St. Clair River, Lake St. Clair, Detroit River System, *J. Hydraul. Eng.*, *136*(8), 507–518, doi:10.1061/(ASCE)HY.1943-7900.0000203.

Austin, J., and S. Colman (2008), A century of temperature variability in Lake Superior, *Limnol. Oceanogr.*, *53*(6), 2724–2730.

Bai, X., J. Wang, D. J. Schwab, Y. Yang, L. Luo, G. A. Leshkevich, and S. Liu (2013), Modeling 1993–2008 climatology of seasonal general circulation and thermal structure in the Great Lakes using FVCOM, *Ocean Modell.*, *65*, 40–63, doi:10.1016/j.ocemod.2013.02.003.

Bartish, T. M. (1984), Thermal stratification in the western basin of Lake Erie, MS thesis, Ohio State Univ., Columbus.

Bartish, T. M. (1987), A review of exchange processes among the three basins of Lake Erie, *J. Great Lakes Res.*, *13*(4), 607–618, doi:10.1016/S0380-1330(87)71676-1.

Beardsley, R. C., C. Chen, and Q. Xu (2013), Coastal flooding in Scituate (MA): A FVCOM study of the 27 December 2010 nor'easter, *J. Geophys. Res. Oceans*, *118*, 6030–6045, doi:10.1002/2013JC008862.

Beletsky, D., and D. J. Schwab (2001), Modeling circulation and thermal structure in Lake Michigan: Annual cycle and interannual variability, *J. Geophys. Res.*, *106*(C9), 19,745–19,771, doi:10.1029/2000JC000691.

Beletsky, D., and D. J. Schwab (2008), Climatological circulation in Lake Michigan, *Geophys. Res. Lett.*, *35*, L21604, doi:10.1029/2008GL035773.

Beletsky, D., J. H. Saylor, and D. J. Schwab (1999), Mean circulation in the Great Lakes, *J. Great Lakes Res.*, *25*(1), 78–93, doi:10.1016/S0380-1330(99)70718-5.

Beletsky D., D. J. Schwab, and M. McCormick (2006), Modeling the 1998–2003 summer circulation and thermal structure in Lake Michigan, *J. Geophys. Res.*, *111*, C10010, doi:10.1029/2005JC003222.

Beletsky, D., N. Hawley, Y. R. Rao, H. A. Vanderploeg, R. Beletsky, D. J. Schwab, and S. A. Ruberg (2012), Summer thermal structure and anticyclonic circulation of Lake Erie, *Geophys. Res. Lett.*, *39*, L06605, doi:10.1029/2012GL051002.

Beletsky, D., N. Hawley, Y. R. Rao (2013), Modeling summer circulation and thermal structure of Lake Erie, *J. Geophys. Res. Oceans*, *118*, 6238–6252, doi:10.1002/2013JC008854.

Bennington, V., G. A. McKinley, N. Kimura, and C. H. Wu (2010), General circulation of Lake superior: Mean, variability, and trends from 1979 to 2006, *J. Geophys. Res.*, *115*, C12015, doi:10.1029/2010JC006261.

Bolsenga, S. J., and C. E. Herdendorf (1993), *Lake Erie and Lake St. Clair Handbook*, pp. 11–229, Wayne State Univ. Press, Detroit.

Boyce, F. M., F. Chiocchio, B. Eid, F. Penicka, and F. Rosa (1980), Hypolimnion flow between the central and eastern basins of Lake Erie during 1977 (interbasin hypolimnion flows), *J. Great Lakes Res.*, *6*(4), 290–306, doi:10.1016/S0380-1330(80)72110-X.

Brant, R., and C. E. Herdendorf (1972), Delineation of Great Lakes estuaries, In *Proc. 15'th Conf. Great Lakes Res.*, pp. 710–718. Internat. Assoc. Great Lakes Res.

Chen, C., R. C. Beardsley, and G. Cowles (2006), An unstructured grid, finite-volume coastal ocean model (FVCOM) system, *Oceanography*, *19*(1), 78–89, doi:10.5670/oceanog.2006.92.

Chen, C., et al. (2007), A finite volume numerical approach for coastal ocean circulation studies: Comparison with finite difference models, *J. Geophys. Res.*, *112*, C03018, doi:10.1029/2006JC003485.

Chen, C., H. Huang, R. C. Beardsley, Q. Xu, R. Limeburner, G. W. Cowles, Y. Sun, J. Qi, and H. Lin (2011), Tidal dynamics in the Gulf of Maine and New England Shelf: An application of FVCOM, *J. Geophys. Res.*, *116*, C12010, doi:10.1029/2011JC007054.

Chiocchio, F. (1981), Lake Erie hypolimnion and mesolimnion flow exchange between central and eastern basins during 1978, *Internal Rep. APSD 9*, Natl. Water Res. Inst., Canada Cent. for Inland Waters, Burlington, Ont.

Côté, J., S. Gravel, A. Méthot, A. Patoine, M. Roch, and A. Staniforth (1998), The operational CMC-MRB global environmental multiscale (GEM) model. Part I: Design considerations and formulation, *Mon. Weather Rev.*, *126*(6), 1373–1395.

Crosby, D. S., L. C. Breaker, and W. H. Gemmill (1993), A proposed definition for vector correlation in geophysics: Theory and application, *J. Atmos. Oceanic Technol.*, *10*, 355–367.

Fay D., and H. Kerslake (2009), *Development of New Stage-Fall-Discharge Equations for The St. Clair and Detroit Rivers*, Int. Upper Great Lakes Study, 48 pp., Environ. Canada Great Lakes Regul. Off. Cornwall, Ont., Canada.

Galperin, B., L. H. Kantha, S. Hassid, and A. Rosati (1988), A quasi-equilibrium turbulent energy model for geophysical flows, *J. Atmos. Sci.*, *45*, 55–62, doi:10.1175/1520-0469(1988)045<0055:AQETEM>2.0.CO;2.

Gedney, R. T., and W. Lick (1972), Wind-driven currents in Lake Erie, *J. Geophys. Res.*, *77*(15), 2714–2723, doi:10.1029/JC077i015p02714.

Haney, R. L. (1991), On the pressure gradient force over steep topography in sigma coordinate ocean models, *J. Phys. Oceanogr.*, *21*(4), 610–619.

Hawley, N., and B. J. Eadie (2007), Observations of sediment transport in Lake Erie during the winter of 2004–2005, *J. Great Lakes Res.*, *33*(4), 816–827.

Kliem, N., and J. D. Pietrzak (1999), On the pressure gradient error in sigma coordinate ocean models: A comparison with a laboratory experiment, *J. Geophys. Res.*, *104*(C12), 29,781–29,799, doi:10.1029/1999JC900188.

Lam, D. C. L., and W. M. Schertzer (1987), Lake Erie thermocline model results: Comparison with 1967–1982 data and relation to anoxic occurrences, *J. Great Lakes Res.*, *13*(4), 757–769, doi:10.1016/S0380-1330(87)71689-X.

Lam, D. C. L., and W. M. Schertzer (Eds.) (1999), *Potential Climate Change Effects on Great Lakes Hydrodynamics and Water Quality*, 232 pp., ASCE, Reston, Va.

León, L. F., J. Imberger, R. E. Smith, R. E. Hecky, D. C. Lam, and W. M. Schertzer (2005), Modeling as a tool for nutrient management in Lake Erie: A hydrodynamics study, *J. Great Lakes Res.*, *31*, 309–318, doi:10.1016/S0380-1330(05)70323-3.

McCormick, M. J., and G. A. Meadows (1988), An intercomparison of four mixed layer models in a shallow inland sea, *J. Geophys. Res.*, *93*(C6), 6774–6788, doi:10.1029/JC093iC06p06774.

Mellor, G. L., and T. Yamada (1982), Development of a turbulence closure model for geophysical fluid problems, *Rev. Geophys.*, *20*(4), 851–875, doi:10.1029/RG020i004p00851.

Mellor G. L., T. Ezer, and L. Y. Oey (1994), The pressure gradient conundrum of sigma coordinate ocean models, *J. Atmos. Oceanic. Technol.*, *11*(4), 1126–1134, doi:10.1175/1520-0426(1994)011<1126:TPGCOS>2.0.CO;2.

Mellor, G. L., L. Y. Oey, and T. Ezer (1998), Sigma coordinate pressure gradient errors and the seamount problem, *J. Atmos. Oceanic. Technol.*, *15*(5), 1122–1131, doi:10.1175/1520-0426(1998)015<1122:SCPGEA>2.0.CO;2.

Mesinger, F., et al. (2006), North American regional reanalysis, *Bull. Am. Meteorol. Soc.*, *87*, 343–360, doi:10.1175/BAMS-87-3-343.

Muth, K. M., D. R. Wolfert, and M. T. Bur (1986), Environmental study of fish spawning and nursery areas in the St. Clair-Detroit River System, *Admin. Rep. 86–6*, U.S. Geol. Surv., Great Lakes Sci. Cent., Ann Arbor, Mich.

Michalak, A. M., et al. (2013), Record-setting algal bloom in Lake Erie caused by agricultural and meteorological trends consistent with expected future conditions, *Proc. Natl. Acad. Sci. U. S. A.*, *110*(16), 6448–6452, doi:10.1073/pnas.1216006110.

Neff, B. P., and J. R. Nicholas (2005), Uncertainty in the Great Lakes water balance, *U.S. Geol. Surv. Sci. Invest. Rep., 2004–5100*, 42 pp.

Quinn, F. H., and E. B. Wylie (1972), Transient Analysis of the Detroit River by the Implicit Method, *Water Resour. Res.*, *8*(6), 1461–1469, doi: 10.1029/WR008i006p01461.

Pedersen, H. H. (2010), Internal pressure gradient errors in sigma-coordinate ocean models: The finite volume and weighted approaches, MS thesis, University of Bergen, Bergen, Norway.

Rao, Y. R., N. Hawley, M. N. Charlton, and W. M. Schertzer (2008), Physical processes and hypoxia in the central basin of Lake Erie, *Limnol. Oceanogr.*, *53*(5), 2007–2020, doi:10.4319/lo.2008.53.5.2007.

Retana, A. G. (2008), Salinity transport in a finite-volume sigma-layer three-dimensional model, PhD thesis, 706 pp., Univ. of New Orleans, New Orleans.

Saylor, J. H., and G. S. Miller (1987), Studies of large-scale currents in Lake Erie, *J. Great Lakes Res.*, *13*(4), 487–514, doi:10.1016/S0380–1330(87)71668-2.

Schertzer, W. M., J. H. Saylor, F. M. Boyce, D. G. Robertson, and F. Rosa (1987), Seasonal thermal cycle of Lake Erie, *J. Great Lakes Res.*, *13*(4), 468–486.

Schwab, D. J. (1978), Simulation and forecasting of Lake Erie storm surges, *Mon. Weather Rev.*, *106*(10), 1476–1487, doi:10.1175/1520-0493(1978)106<1476:SAFOLE>2.0.CO;2.

Schwab, D. J., and K. W. Bedford (1994), Initial implementation of the great lakes forecasting system: A real-time system for predicting lake circulation and thermal structure, *Water Qual. Res. J. Can.*, *29*(2–3), 203–220.

Schwab, D. J., D. Beletsky, J. DePinto, and M. Dolan (2009), A hydrodynamic approach to modeling phosphorus distribution in Lake Erie, *J. Great Lakes Res.*, *35*(1), 50–60.

Shore, J. A. (2009), Modelling the circulation and exchange of Kingston Basin and Lake Ontario with FVCOM, *Ocean Modell.*, *30*, 106–114, doi:10.1016/j.ocemod.2009.06.007.

Smagorinsky, J. (1963), General circulation experiments with the primitive equations. 1: The basic experiment, *Mon. Weather Rev.*, *91*(3), 99–164, doi:10.1175/1520-0493(1963)091<0099:GCEWTP>2.3.CO;2.

Wilson, M. C., J. A. Shore, and Y. R. Rao (2013), Sensitivity of the simulated Kingston Basin—Lake Ontario summer temperature profile using FVCOM, *Atmos. Ocean*, *51*(3), 319–331, doi:10.1080/07055900.2013.800017.